Article:
Isaac, O.S., Alshammari, O.G., Pickering, E.G. et al. (2023) Blast wave interaction with structures – an overview. International Journal of Protective Structures, 14 (4). pp. 584-630. ISSN: 2041-4196

https://doi.org/10.1177/20414196221118595

Review

International Journal of
Protective Structures

Blast wave interaction with structures – An overview

International Journal of Protective Structures
2022, Vol. 0(0) 1–47

DOI: 10.1177/20414196221118595
journals.sagepub.com/home/prs

Obed Samuelraj Isaac, Omar Ghareeb Alshammari, Erik Green Pickering, Samuel David Clarke and Samuel Edward Rigby

Abstract

Blast–obstacle interaction is a complex, multi-faceted problem. Whilst engineering-level tools exist for predicting blast parameters (e.g. peak pressure, impulse and loading duration) in geometrically simple settings, a blast wave is fundamentally altered upon interaction with an object in its path, and hence, the loading parameters are themselves affected. This article presents a comprehensive review of key research in this area. The review is formed of five main parts, each describing: the direct loading of a blast wave on the surface of a finite-sized structure; the modified pressure of the blast wave in the wake region of three main obstacle types – blast walls, obstacles, wall/obstacle hybrids; and finally, a brief description of some methods for predicting loading parameters in such blast–obstacle interaction settings. Key findings relate to the mechanisms governing blast attenuation, for example, diffraction, reflection (diverting away from the target structure), expansion/volume increase, vortex creation/growth, as well as obstacle properties influencing these, such as porosity (blockage ratio), obstacle shape, number of obstacles/rows, arrangement and surface roughness.

Keywords

Blast wave interaction, blast wave attenuation, clearing, blast wave simulation, fast-running methods

Introduction

The loads on a structure as a result of a high explosive detonation can be due to (i) the impact of the shock wave and the drag force from the blast wave, (ii) the impact of the flying debris set in motion by the wind behind the shock wave (Gebbeken et al., 2017) and/or (iii) due to the ground shock (Barakat and Hetherington, 1999; Beshara, 1994b). In this article, we present a comprehensive

Department of Civil and Structural Engineering, The University of Sheffield, Sheffield, UK

Corresponding author:
Obed Isaac, Department of Civil and Structural Engineering, The University of Sheffield, Sheffield S10 2TN, UK.
Email: obed.isaac@gmail.com

overview of recent literature on the first aspect, restricting this to address aspects pertaining to (air) pressure loading on a structure.

Early research on blast loading studies predominantly reports the use of high explosives in the range of kt or Mt TNT equivalent to replicate the effects of a nuclear explosion (Beshara, 1994a). Therefore, blast effects were typically measured at stand-off distances that were hundreds of metres away (Biggs, 1964; Norris et al., 1959). This would allow for sufficient time for the spherical shock front to transition into a planar wave relative to the size of the domestic homes, nuclear shelters, etc. that were usually tested (illustrated at time t_4 in Figure 1(a)). Under such conditions, relatively simple semi-empirical methods found in blast textbooks (Hyde, 1991; Kingery and Bulmash, 1984; Kinney, 1985) could be made use of to obtain the total loading on the structures. Further details on such formulations may be found in the review by Beshara (1994a, 1994b).

Over the last few decades, however, an increase in terrorist activity has led to blast loading and blast resilient design becoming an increasing aspect of modern structural engineering. This was not only for high risk buildings (FEMA, 2007; Remennikov, 2003) but also for 'soft' civilian infrastructure. In a congested urban environment, where the explosives are more likely than not to be set-off on a street, or in a parking lot, the shock wave radii on impact would be comparable to the dimensions of the structure itself. For such conditions, the use of simplifying assumptions for estimating the load over the entire building would no longer be possible. Instead, a spatially varying, time-dependent pressure value would have to be evaluated at each point on the structure (e.g. at time t_1 in Figure 1(a)). This level of detail is necessary to arrive at a more effective and efficient design for such non-planar loads. It is therefore clear that depending on the stand-off distance and the relative size of the building, we can have different scenarios for the evaluation of blast loads, ranging from very simple cases to complex ones. It is also common in blast resilient design to incorporate passive

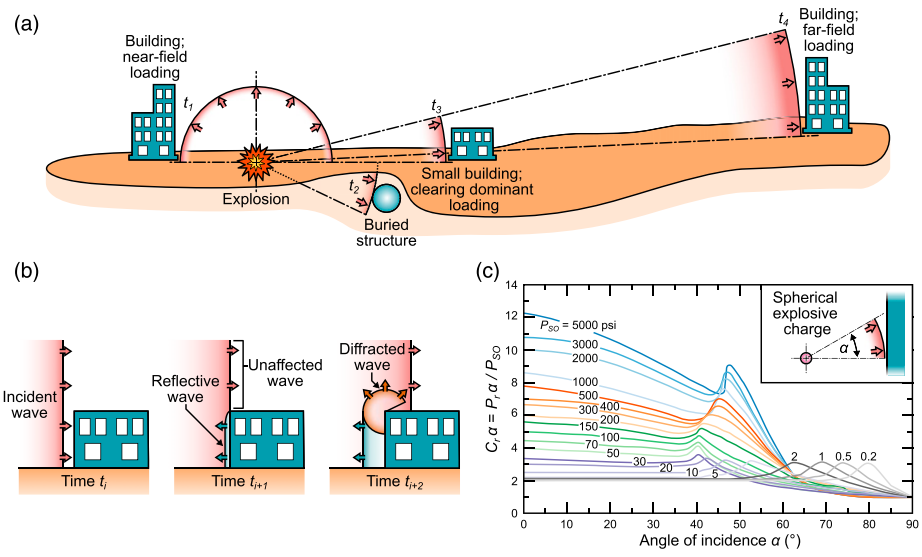

Figure 1. (a) An illustration demonstrating the different loading types resulting from a single explosion as a function of their stand-off distance and building size. (b) A schematic representation of the development of the clearing effect on a small building. (c) Graph illustrating the effect of the angle of incidence(α) of the blast on the reflection coefficient C_r of a building structure (Kinney 1985).

techniques to ameliorate the blast load on a structure by modifying the blast wave itself and/or the nature of its interaction with a structure.

In this paper, we thus present an overview of research on characterizing the blast overpressure load given the size and shape of a structure and its distance from the site of the explosion and the mitigation of this pressure load using passive techniques that depend on the shape/external profile of the structure. This article has hence been organized as below:

- First, aspects pertaining to direct blast loading on structures of various shapes are addressed.
- The next three sections cover the (indirect) loading of a planar surface after the incident blast wave has interacted with one of these:

(i) *Quasi-2D wall-like structures/barriers*, where the length of the barrier (running perpendicular to the direction of the blast wave) exceeds the height. The length and height surpass the depth of the structure.
(ii) *Quasi-1D pole-like structures/obstacles*, where one dimension of the structure (typically the height) exceeds the other two dimensions.
(iii) Combinations of type *(i)* and *(ii)*, which we term here as *hybrids.*

- Finally, a section containing a brief description of the methods and tools that are available to estimate the loads on a structure following a direct or indirect blast event has been included for completeness.

General considerations

As the shock front advances from the source, the explosion energy is rapidly distributed over an increasingly larger volume, leading to a reduction in the peak overpressure p_s and the impulse of the blast wave I_s.[1] An illustration demonstrating such a decay of pressure values along a radial line from the centre of the explosion, at different time instances, may be seen in Figure 2(a). At each point in the affected region, following the initial pressure jump, the blast pressure exponentially decays and undershoots below the ambient values, and then recovers comparatively slowly. This demarcates the positive and negative phases of the blast wave as depicted in Figure 2(b). It is worth noting that the 'shock wave' refers to the infinitesimal region across which the pressure increases instantaneously, whereas the 'blast wave' is the entire region over which the blast wind acts (Figure 2(b)).

On interacting with a rigid surface, the shock pressure enhances owing to the drop in the kinetic energy of the air molecules. This enhancement, called reflected overpressure p_r, depends on the compliance of the surface, and the incident angle α at which the shock wave impinges the surface. It is also influenced by the value of the incident pressure itself as shock wave reflection, unlike acoustic wave reflection, is a highly non-linear process.[2] These reflected pressure values may be obtained (Kinney 1985) in terms of the reflection coefficient, C_r, as shown in Figure 1(c). It is to be noted that the use of the term overpressure is preferred in blast literature as the pressure difference from the ambient level is what causes damage to structures (Needham, 2010). For the sake of convenience, in this article, 'overpressure' has been used only where the meaning is not clear.

Types of Loading: The major contribution to the total blast load on a building arises from the front face (Glasstone and Dolan, 1977; Gauch et al., 2019), and so this review focuses mostly on frontal loads. On the front face of a structure being impacted by a blast wave, the pressure instantly rises to the said reflected value p_r, and then begins to decay at a rate that initially depends on the intensity of the blast itself, and also on the shape and size of the structure. The wave then progressively loads the side walls and subsequently the rear portion of the structure, eventually engulfing the entire unit.

This entire process is referred to as diffraction loading (Norris et al., 1959). After the passage of the shock wave, (the momentum of) the blast wind loads the structure, and the stagnation pressure (p_0, see Figure 3), which is the sum of the static blast load p_s and the drag coefficient C_D[3] multiplied by the dynamic pressure q_s, causes drag loading on the structure. The negative phase of the blast wind then exerts a load on the structure in the opposite direction of the initial blast load.

While diffraction loading is relevant for short duration blast waves, drag loading, on the other hand, is the dominant contributor to the total load for longer duration blasts commonly encountered in atomic and nuclear explosions. The negative phase load, although typically much lower, can still influence structural response. It can be highly relevant for flexible structures (Rigby et al., 2017b) based on relative values of the decay time of the blast load and the response time of the structure. Nevertheless, to keep things simple, the contribution of the negative phase to the total load has been excluded from the scope of this review.

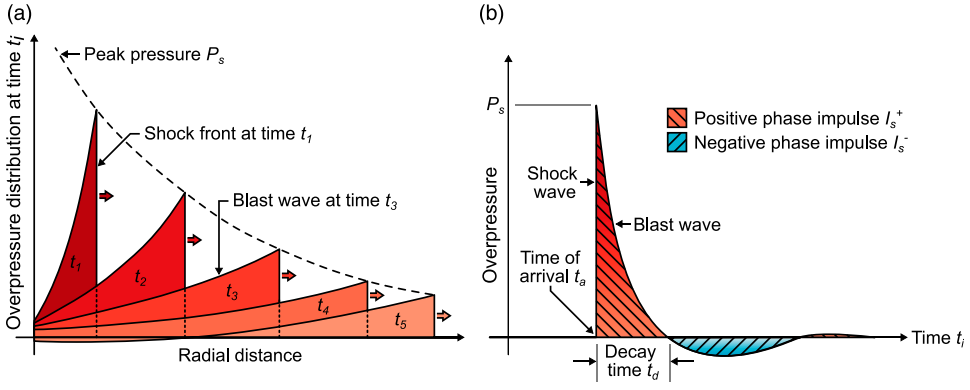

Figure 2. A graphical representation of the overpressure evolution resulting from a blast wave shown (a) spatially at a given time t_i and (b) temporally at a fixed point.

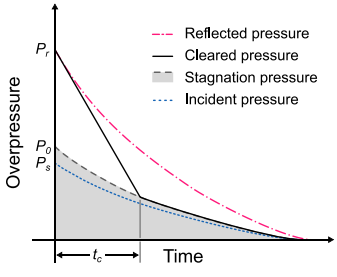

Figure 3. A graphical representation of the different transient pressure histories encountered in blast interaction with structures; incident/static pressure P_s, reflected pressure P_r, stagnation pressure P_0 and cleared pressure. The reduction in pressure loading due to clearing in the time period t_c is clearly illustrated.

Direct loading on a structure

Clearing mechanism

As mentioned previously, the front face of a structure loaded by a blast wave experiences a reduction in the magnitude of pressure due to the shape of the structure. This phenomenon, which is in addition to the free-field blast pressure decay, is termed as 'clearing' (Figure 1(b)) and this occurs due to the presence of the free edges in a finite-sized structure. The peak reflected overpressure p_r of the blast load, however,[4] does not change as the reflection of an incident blast wave is effectively instantaneous and is unaffected by clearing (Mulligan, 2018).

Now, consider a finite-sized structure such as a cuboid being impacted by a blast (Figure 1(b)). As soon as the shock front impacts a point (or region[5]) on the front face of the cuboid, it reflects, leading to a sudden increase in pressure at that point (or region). On reflection, the direction of travel of this disturbed portion of the wave reverses, whereas in the surroundings of the cuboid, the undisturbed blast front continues to travel ahead, unimpeded. There is thus a pressure discontinuity that propagates inwards from the edges of the cuboid, leading to the formation of an expansion wave to counteract the pressure gradient. Unlike the discontinuous and sudden nature of the shock wave, the expansion wave is a continuous, acoustic wave (Liepmann and Roshko, 2013). Therefore, the reflected pressure is lowered progressively over the front face of the cuboid, starting from the edges and then to the centre. Relative to the air velocity behind the reflected wave, the expansion (clearing) wave travels at the local sound speed. The air velocity in the reflected region being usually negligible, especially for cases where the incident and the reflected waves are planar with no other disturbances, the clearing wave can propagate quite quickly. This leads to a substantial reduction in pressure on the face of such finite object (Rigby et al., 2014b; Tyas et al., 2011) during the 'clearing time' t_c as illustrated in Figure 3. At the end of this clearing phase, the pressure is usually taken to follow the stagnation pressure p_0.

Special Case 1: Infinitesimal and infinite size structures

A simple scenario presents itself when the frontal portion of the structure itself can be considered small enough, relative to the radius of the wave, to resemble a point. For such a case, the incident free-field values of pressure and impulse (Kinney, 1985; Kingery and Bulmash, 1984; Hyde, 1991) may be readily used to obtain the loading on the structure.[6] This is because the clearing time t_c is effectively *zero* and the cross-section area to resist the flow and attain stagnation pressure p_0 is also minuscule for such structures (cf., Figure 3).

The other extreme would be a case where the structure is infinitely large, such as the floor/ground being impacted by an air blast, leading to a complete wave reflection off the surface. The loading parameters for such a scenario would then be the ideal peak reflected overpressure and impulse values. These may be determined from standard semi-empirical methodologies (Kinney, 1985; Kingery and Bulmash, 1984; Hyde, 1991), or from the incident pressure charts in conjunction with a ground interaction parameter (Baker, 1973) or a reflection coefficient (Figure 1(c)).

Special Case 2: Finite target sizes, longer stand-off distances

For the case illustrated at time t_3 in Figure 1, where the explosion occurs at a large distance from the target structure and the distance from the edges to the centre of the target object is small relative to the stand-off distance, clearing is said to occur 'completely'. This is when the clearing wave

completes traversing the half-width of the structure much before the completion of the (undisturbed) blast loading phase. Under such circumstances, the clearing wave can therefore counteract and almost completely negate the increase in pressure due to reflection. This can lead to an almost undisturbed state of the blast wave (with 'clearing time' $t_c \sim 0$, see Figure 3) for such structures.

This is a reasonable expectation for structures subjected to a large-scale explosion, where the blast duration is quite long (thousands of milliseconds), and the clearing wave can quickly traverse the face of the structure (a few milliseconds). For larger structures, however, assuming that an undisturbed state exists throughout the face of the structure is not valid. Nonetheless, for such cases, one may expect the clearing to begin simultaneously at all points on the face of the target. It is then sufficient to obtain a single characteristic 'clearing time' t_c for the entire structure. Over this time t_c, the overpressure may be taken to drop linearly from the peak reflected pressure p_r to the stagnation pressure p_0 as shown in Figure 3. In other words, for this special case, even if the values cannot be read off directly from a chart, a single pressure trace may be easily constructed to estimate the load over the entire front face of the structure. To estimate the clearing time, several formulae, which are essentially variations of equation (1), are available, as proposed by Kinney (1985), and UFC 3-340-02 (US Department of Defence, 2008)

$$t_c = \frac{\text{Representative Clearing Dimension}}{\text{Representative Velocity}} \tag{1}$$

This methodology has been numerically validated (Rigby et al., 2014b) for cases where the representative dimensions of the object, S, are much lower than the scaled stand-off distance,[7] that is, $S << Z$. For relatively small buildings with $S/Z << 1$, as mentioned earlier, the clearing time is often negligible compared to the blast duration, and the loading essentially follows the incident pressure curve if the drag load is negligible. Thus, when the loading of the structure is in the impulsive regime, the *incident* impulse data would suffice to predict the response of these structures. The use of SDOF methods (Biggs, 1964; US Department of Defence, 2008) can then offer a means to quickly and reliably design simple structures for direct loading scenarios (Rigby et al., 2013). However, it is not always straightforward to obtain the loading curve for other complex scenarios.

Finite target sizes, comparable stand-off distances

Due to an increase in terrorist activity in the last few decades, the research focus has shifted from blast load estimates on isolated small shelters to that on modern buildings in an urban setting. Here, the scaled sizes of the target structures such as buildings, shopping malls and stadia would be comparable to the scaled distance from the explosive. This is because, in urban terrorism, the use of explosives ranging from 5 to 1000 kg, at stand-off distances of just a few metres is commonplace. For these conditions, one can no longer assume clearing effects to equalize quickly relative to the duration of the blast wave. For example, Rose et al. (2006) numerically demonstrated that clearing waves are initiated from different free edges at different times when an explosion occurs at an oblique angle to a tall building, which will render the simple relations incorrect. And so each point on the face of the target will have a unique pressure trace, thereby rendering the previous methods unsuitable as they would be highly conservative (Rigby et al., 2013). While clearing always implies a reduction in the blast wave pressure, Rigby et al. (2012, 2014a) used an SDOF model to demonstrate that clearing can produce a counter-intuitively higher displacement for certain t_d/T_n ratios. Thus, to obtain the final response of the structure whose dynamic aspects cannot be

neglected, a holistic view needs to be adopted towards understanding the clearing response. However, estimating the response of the structure is beyond the scope of this article.

In the following sub-sections, we report studies on clearing loads on objects of different shapes under the following headings:

- Obstacles with straight faces and
- Obstacles with curved faces.

Obstacles with straight surfaces. Several researchers have studied the role of clearing over the last few decades, primarily to understand the limitations of the extant simplified models that were previously described. New models were then proposed, which are mostly valid only for a planar wave impacting a structure. Essentially, the proposed methods attempt to approximate the start time of clearing at each point, and then the deviation from the non-cleared (reflected) pressure is predicted in terms of a relief function (Rigby et al., 2013), or Hudson parameter (Rigby et al., 2014b; Tyas et al., 2011), or a Friedlander profile (Qasrawi and Heffernan, 2016). This concept of tracking the deviation from the reflected pressure is a noticeable shift from the earlier methods, where reliance on stagnation pressure as the baseline value was paramount.

Rickman and Murrell (2006) explored the validity of the simple clearing formulas (equation (1)) for a box-shaped structure whose dimensions were comparable to the stand-off distance. Experiments were conducted using C4 explosive on two structures having dimensions of 0.33 × 0.33 × 0.46 m and 0.572 × 0.572 × 0.737 m. A 92 g TNT equivalent charge was used at $0.323 < Z < 9.11$ m/kg$^{1/3}$ and $0.54 < Z < 5.35$ m/kg$^{1/3}$ for the smaller and the larger structure, respectively. They reported clearing pressures on the face of the structure (for $Z > 1.8$ m/kg$^{1/3}$) that were far lower than the stagnation pressures, which was contrary to the conventional thinking of that day. They concurred that this may be due to the disturbance introduced in the flow field by the structure. To account for this experimental finding into a model for the clearing pressure, the authors then proposed a relief function, defined as the difference between the actual pressure on the face of a structure and the un-cleared (ConWep) reflected pressure value. Now, to use the relief function, the time instant from which the pressure starts deviating from the ConWep value is required. For this, they proposed the use of an empirical formula for the velocity of the clearing wave from which the clearing initiation time may be obtained. The empirical relief function was then successfully validated for stand-off distances ranging from 0.82 m to 5.5 m for a 92 g TNT equivalent charge.

Tyas et al. (2011) show how clearing reduces the average impulse over a finite-sized target when the stand-off distances are increased ($Z = 6$–14.9 m/kg$^{1/3}$). They then proposed a method to calculate the load on a finite-sized object, similar to the methodology adopted by Rickman and Murrell (2006). Essentially, this method was based on the work of Hudson (1955) that had largely been overlooked. Hudson's method was used to account for waves arriving at a given point from each edge, which were then combined using simple linear superposition. Excellent agreement with experimental data was found as shown in Figure 4. The authors suggest that the overestimated pressure drop seen in the latter stages could be the result of the simplifying assumptions that were used, viz., Hudson's method to calculate speed, and the use of linear superposition. Overall, the prediction of the clearing was seen to improve with increasing stand-off distance as the wave tended towards becoming a weak, planar shock. This modified Hudson's approach was later validated using large-scale test data as well (Rigby et al., 2017a). Here again, it is worth noticing in Figure 4 that the pressure, on completion of clearing, does not follow the stagnation pressure as had been originally postulated.

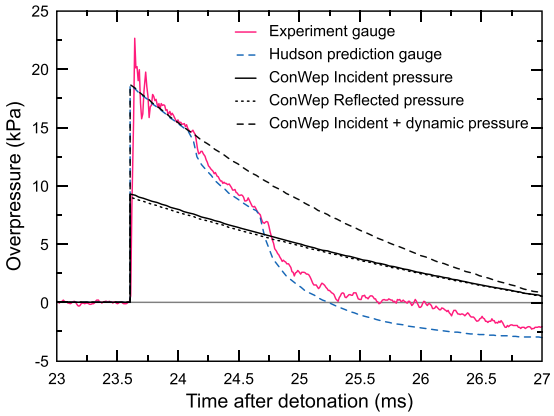

Figure 4. A plot showing the results of the method proposed by Tyas et al. (2011) to obtain cleared pressure, compared against experimental data and simplified ConWep based approximations.

Subsequent to the experimental validation by Tyas et al. (2011), Rigby et al. (2014b) presented a refined version of the Hudson (1955) clearing theory. They showed for conditions typical of far-field ($Z = 8$ m/kg$^{1/3}$), that is, a weak, planar shock, that diffraction waves do not repeatedly travel along the face of the obstacle until equilibrium is achieved. Instead, the clearing wave traverses the face of the target just once. Then, subject to favourable conditions, it reflects off the ground (or another shock from the opposite edge) and transverses along the face once again and finally escapes into the surrounding volume. They also reviewed different methods of estimating clearing against a validated LS-Dyna model for objects of different heights, S, ranging from $Z/256$ to $Z/32$. The Hudson method was found to be excellent at predicting the loading on the front face of a finite-sized cuboid. Incidentally, they also show that a commonly used simple prediction model based on equation (1) (described in detail later, see equation (6)) is valid for building sizes that are much smaller than the scaled distance ($S \ll Z$). This shows that the simple model is valid for predominately drag-type loading, whereas the Hudson model works for both diffraction and drag-type loading at these ranges of pressures. Having observed increasing over-expansion of the pressure, that is, cleared overpressure dropping below the stagnation pressure for larger structures, the authors report that the extent of over-expansion of the air could be connected to the size of the structure itself.

Since the aforementioned models are valid for only far-field Z values (Rigby et al., 2014b; Tyas et al., 2011), an improved scheme that could also account for stronger shocks ($1 < Z < 5$ m/kg$^{1/3}$) was proposed by Qasrawi and Heffernan (2016). Simulations were carried out to study the clearing on the circular, flat face of a cylinder of radius 500 mm, at three stand-off distances (D=10, 25, 50 m). For each stand-off distance, three different scaled distances (Z=1, 2.5, 5 m/kg$^{1/3}$) were used, each of which were chosen to ensure planarity of the wave impacting the front face. They found the speed of the clearing wave to be a constant value close to the local speed of sound for each scaled distance. They then developed and validated an empirical Friedlander-type wave profile to estimate the effect of clearing at each point on the front face of a finite cuboidal target (Figure 5). The authors attribute the slight discrepancy in the plots to the fact that the clearing waves are different for a cylindrical (for which the model was developed) and a cuboidal obstacle (against which it was tested). Unlike the earlier studies, here they found that on completion of clearing, the pressure followed the stagnation pressure values for all but few cases – $D = 10$ m, $Z = 2.5$ and 5 m/kg$^{1/3}$ and $D = 25$ m, $Z = 5$ m/kg$^{1/3}$.

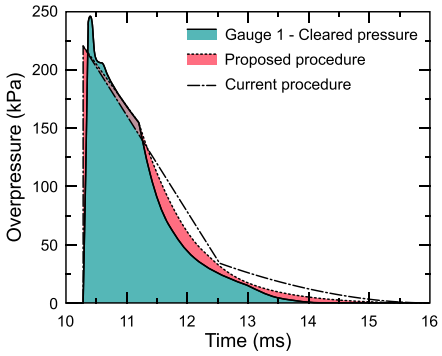

Figure 5. The procedure proposed by Qasrawi and Heffernan (2016) to model the clearing effect for a *cylindrical model* validated against numerical data (gauge 1) for a *cuboidal obstacle*. The pressure curve from a simple clearing model (standard text book procedure) has been included for reference. Figure reworked from Qasrawi and Heffernan (2016).

All these cases have scaled radius of the cylinder lower than $Z/20$. It thus appears that the threshold of validity of the simple UFC models for the closer stand-off distance scenario is different from the $Z/256$ for the far-field (Rigby et al., 2014b). Combining this with the observation by Rigby et al. (2014b) regarding the over-expansion of the flow, it seems that the disturbance introduced by an object in a high-speed flow (small values of Z) is much lesser than that introduced by a similar sized object in a lower speed flow (bigger values of Z). This has potential ramifications on the sizing of structures for blast mitigation in the downstream (wake) region, depending on the scaled stand-off distance Z.

Recently, a comprehensive semi-analytical method to obtain the total force on a 2D object by using overpressure histories on the front and rear face of the object was proposed by Gauch et al. (2019). This method was primarily intended for deflagration loading and for low intensity blast loading. So the blast parameters that were considered range from an incident overpressure of 1 bar and 10 ms decay time to 3 bar and 1 ms decay time for a box height of 346 mm and ambient conditions of 1 bar, 15°C. The method has been numerically validated and several inferences on the rise time of the total force on the front face, the rear face and the relative contribution of different physical phenomenon to the total force term have been made available.

For scenarios where the loading is not at *zero* angle of incidence, an empirical formula in terms of the angle of incidence and the energy of the explosion were provided to estimate the pressure load on a 3D box structure by Trélat et al. (2007). This was based on experiments using an explosive gaseous charge and a parallelepiped structure of dimensions $0.14 \times 0.18 \times 0.4$ m ($W \times H \times D$). The TNT equivalent masses ranged from 0.159 to 2.023 g at stand-off distances of 0.1 m–0.2 m. The box was positioned at 5 different angles (0, 30, 45, 60 and 90°) with respect to the charge. Here, the first and last case involved the box being positioned perpendicular to the small face and the large face, respectively. It is worth reiterating that all the aforementioned predictive models assume an impingement of a planar wave and usually correspond to the far-field, where clearing plays a prominent role.

For the near-field ($0.2 < Z < 3$ m/kg$^{1/3}$), Shin and Whittaker (2019) present a comparison of a validated AUTODYN simulation against the simple clearing formulae and demonstrate their inaccuracy in the near-field. In addition to that, using plots of the particle velocity along the front face of the object (Figure 6), they suggest that clearing cannot occur in the near-field as the expansion

wave is prevented from travelling inwards. This is due to the particle speeds being higher than the local sound speed. They also go on to show that predicting clearing for these conditions is made difficult by the variability of the particle speed along the face of the object. This is more so when the wave is not planar. As an aside, one may note that the speeds are more or less constant for $Z > 1$ m/kg$^{1/3}$ as reported by Qasrawi and Heffernan (2016). For non-planar, close range blast loads, they therefore suggest the use of CFD tools to estimate clearing loads.

Obstacles with curved surfaces. For obstacles with curved surfaces, one major difference is that the clearing load is further reduced because of the relieving effect provided by the three-dimensional nature of the surface. For simple loading cases, viz., far-field of large (> 0.1 MT of TNT) explosions, for a spherical dome and for structures with simple curved surfaces, load estimation formulae are available in textbooks (Biggs, 1964; Norris et al., 1959; Glasstone and Dolan, 1977). These predictions are not applicable for smaller charges, and recently, Qi et al. (2020) quantified the inaccuracy in using existing conventional models (e.g. UFC 3-340-02) to obtain overpressures on a hemispherical dome. This formula uses scaled distance and inclination angle at a location on the dome as inputs. Discrepancies of up to −150% for overpressure and up to −90% for impulse were reported, as clearing plays an important role in this reduction (Qi et al., 2020). Thus, load estimation on curved surfaces for such blast parameters has been an ongoing area of research in the last few years.

Due to a lack of experimental data for curved faces of structural columns, Shi et al. (2007) report numerical studies on columns loaded by blast waves at scaled distances ranging from $Z = 0.5$ to 10 m/kg$^{1/3}$. For rectangular columns, they found that the peak overpressure and impulse at a point on the front face of the column were not affected by the depth of the column. But then, the reduction was inversely proportional to the width of the column, until an asymptotic limit was reached at 1.6 m. For a circular column, a similar limit was reached at 3 m diameter. For the pressure evolution on the rear face, the width of the column had a stronger effect than the depth. The reflection off the rectangular column was stronger, whereas the diffracted wave was stronger on the rear face of the circular column. They also report an anomalous increase in reflected impulse at 1/3rd the height of the column for $Z < 1$ m/kg$^{1/3}$ which they attribute to a combination of shock reflection off the ground and deflection of the column, both of which increase the positive pulse duration. Empirical predictions for the overpressure and impulse on the front and rear faces along the column height were made in terms of the respective values at the base of the column, which were again obtained empirically.

Since depth does not appear to play an important role, this work can be compared with the work of Ballantyne et al. (2010) who studied the role of clearing in reducing the impulse on the flange face of commonly used structural W-sections (wide-flange sections, also called H-sections). Parametric numerical studies were carried out for values of Z between 2 and 10 m/kg$^{1/3}$ and they report that the impulse reduction due to clearing tends to be essentially constant for these flange sections. The constant value was found to be 50% of the reflected impulse on an infinite surface. The authors then derived an empirical formula to estimate the impulse for $Z = 1$–10 m/kg$^{1/3}$. These results are for the impulse values on the front face alone.

Glasstone and Dolan (1977) provide relations for estimating the area-averaged overpressure history on the front, sides and rear face of a cylinder for the case of planar loading and $Z > 3$. After this, in the last decade, several numerical and experimental works were carried out to improve on these highly conservative estimates.

Qasrawi et al. (2015) used numerical simulations to study the development of pressure on a circular section. The cylinder radii ranged from 0.1 m to 1.0 m, the stand-off distance was 2 m and

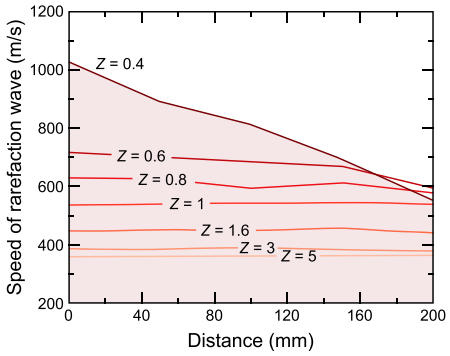

Figure 6. A plot showing the variation of rarefaction (clearing) wave speed for different scaled blast values (Z, kg/m$^{1/3}$) along the face of a target as a function of the distance from the centre of the target (Shin and Whittaker, 2019).

the scaled distances were from $Z = 0.8$ m/kg$^{1/3}$ to 2.4 m/kg$^{1/3}$. The variation around the cylinder was found to be well represented by a sinusoidal function, and they then derived the following expressions for predicting overpressure (equation (2)) and impulse (equation (3)) acting on the circular column

$$P_{equiv} = \frac{2}{3\pi}[2P_r + P_{so}] \tag{2}$$

$$I_{equiv} = \frac{2}{3\pi}[2I_r + I_{so}] \tag{3}$$

For columns of large radii, they recommend the use of incident blast parameters (P_{so} and I_{so}) at the side of the cylinder, as the cylinder radius can add to the stand-off distance from the charge and lead to incorrect results. These formulas are an improved yet conservative estimate that may be used for preliminary design calculations for circular columns.

While Qasrawi et al. (2015) had neglected the overpressure on the rear surface of the cylinder as they were interested in providing a conservative estimate, Mulligan (2018) provides some empirical relations for the front and rear face of a circular cylinder for similar scaled ranges, based on small-scale experiments. C4 charges ranging from 0.09 kg to 0.272 kg, placed at a stand-off distance of 1.32 m from a 167 mm diameter cylinder, were used in these experiments (the reflected overpressures were in the range of 3–9.5 bar). The empirical relations were provided as a function of the azimuth angle, giving improved prediction values over that given previously by Glasstone and Dolan (1977). Beyond the 90° azimuth, they found that turbulence and surface roughness on the cylinder play an important role in the overpressure evolution over the cylinder.

Experiments have also been reported on a hemi-cylindrical obstacle to simulate conditions over a transport cask/industrial facility (Trélat et al., 2020). To do so, the obstacle was positioned so that the 0.4 m diameter hemi-cylinder's axis that was 1.6 m long was perpendicular to the direction of propagation of the blast wave. For these experiments, a 50 g equivalent TNT charge was used at three different stand-off distances – 0.4, 0.6 and 1.6 m. The pressure enhancement measured along the front face of the cylinder could be predicted quite successfully by TM5-1300 (US Army Corps of Engineers, 1990) using the reflection model for a plane target. However, the drop in pressure in the

expansion region of the cylinder could not be predicted as this includes complex diffraction effects. And so, an empirical model (called *Model S*) was proposed for predicting the overpressure values in the expansion region with the help of a modified coordinate system. This model was then successfully validated against a factor two scaled-up experiment.

The overpressure evolution on a perfectly hemispherical dome having a rise to span ratio, f/L = 0.5 (Figure 7(a)) was experimentally studied for Z = 1.7–3.4 m/kg$^{1/3}$ (see Table 1) by Zhi et al. (2019). The authors performed numerical simulations for a wide range of parameters and developed empirical formulae for blast parameters such as the reflected pressure, impulse and decay time. This was for points over the surface of the hemisphere as a function of the span of the hemisphere and the scaled distance from the charge. In an interesting finding, pressure values at points on the hemisphere along a direction perpendicular to the blast wave and away from the centreline were found to be the same. This was named by the authors as the *parallel effect*.

Extending these tests further, Qi et al. (2020) carried out experiments for this and another hemispherical dome having a rise to span ratio, f/L, of 0.22 (Figure 7(b)) with a taller cylindrical base. This was done for Z ranging from 1.2 to 3.7 m/kg$^{1/3}$ to study the effect of the height of the supporting base and the new rise to span ratio. Using a numerical parametric study, and they identified the following dimensionless variables – scaled span $L/W^{1/3}$, distance-span ratio R/L, rise-span ratio f/L and height-span ratio H/L as important parameters in the loading process. Then, empirical formulas to predict the blast load on the structure were obtained and were validated fairly successfully.

Buildings in urban scenarios: Simulations and experiments

To study the overpressure load on actual building shapes, there is a relative dearth of data in the literature apart from the simple structures described thus far. As load relieving aspects of curved surfaces were recognized early by Barakat and Hetherington (1998), shapes that an architect may use to minimize the loading on a building were explored and identified. On the whole, structures with curved surfaces were found to have a reduced magnitude of the imparted blast load as the reflected waves can then be directed away from the structure. Provisions for such a design were incorporated in the design of a new building (US General Services Administration, 2004) to replace the damaged Alfred P. Murrah building and similar examples of such buildings may be found in the FEMA (2007) design manual. Convex building façade shapes are usually preferred for blast resilient design with a view to avoid wave reflection hotspots (US Army Corps of Engineers, 1990). To illustrate, a building designed as shown in Figure 8(a) is to be avoided, whereas the design ought to be as recommended in Figure 8(b). But then, Gebbeken and Döge (2010), using CFD simulations, show how an intelligently designed non-convex shape (Figure 8(c)) can also lead to a reduction in blast pressure loading on the building structure.

To understand the effect of building design parameters such as the overhang of the roof of a gable roof building, Xiao et al. (2021) report experiments for two different loading scenarios, one on the eave side and the other on the gable side, as shown in Figure 9. An LS-Dyna numerical model was initially validated against 4 experiments at different scaled distances; some facing the gable side, and some facing the eave side of the building. Following this, a numerical parametric study on the building design parameters was carried out. They found that an overhang in the roof led to an increase in the pressure and impulse on the (side) wall. The overpressure was found to increase with increasing roof overhang and roof slope. On the other hand, the impulse increased with roof overhang but remained unaffected by a change in the slope of the roof.

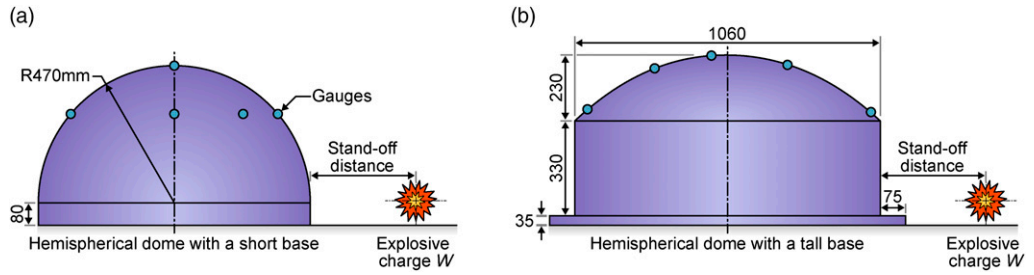

Figure 7. A schematic drawing of the hemispherical dome setups used by (a) Zhi et al. (2019) and (b) Qi et al. (2020) to investigate the variation in pressure development on a curved surface.

Table 1. Summary of literature on predicting blast loading on objects with curved surfaces.

Structure shape	Representative scale	TNT Eq. weight (or incident pressure)	Stand-off distance (or decay time)	Loading estimates
Circular and square column (Shi et al., 2007)	ϕ 500–ϕ 3000 mm	1–8000 kg	10 m	Empirical
Cylinder and flat plate (Mulligan, 2018)	ϕ 168 mm	0.09–0.27 kg	1.32 m	Empirical
Hemi-cylinder (Trélat et al., 2020)	ϕ 400 mm × 3.2 *m*	0.05 kg	0.4–1.6 m	Empirical
"	ϕ 800 mm × 3.2 m	0.4 kg	3.2 m	"
Hemisphere (Zhi et al., 2019)	ϕ 940 *mm* (f/L=0.5)	0.055–0.4 kg	1, 2 m	Pseudo-analytical formula
Hemisphere (Qi et al., 2020)	ϕ 940 *mm* (f/L=0.5)	0.055–0.4 kg	1, 2 m	Pseudo-analytical formula
"	ϕ 1060 *mm* (f/L=0.217)	0.055–0.4 kg	1, 2 m	Pseudo-analytical formula

The role played by the landscape ahead of a building in modifying the blast load even before it impacts a building was numerically investigated by Barakat and Hetherington (1999). They show how careful planning of landscaping in the regions surrounding the building, illustrated in Figure 10, can help reduce the blast intensity. Pits, trenches and humps are another elegant method to reduce the load in the framework of architectural design. The TNT charge mass that was used for these simulations was not mentioned, but the study aimed at evaluating vehicle bomb threats (25 – 230 kg TNT) at distances ranging from 20 to 50 m. Reductions of up to 35% on impulse, and up to 40% on pressure, were shown to be possible by employing such techniques (Barakat and Hetherington, 1999).

While all these are studies on different aspects of blast loading on a stand-alone building, the design loads will be different for buildings in an urban, congested environment. Additional factors which can modify the evolution of pressure loading such as the width of the street, building height, the type of façade and the presence of openings in the building envelope ought to be taken into consideration. Recent large-scale blast events such as the 2020 Port of Beirut explosion (Rigby

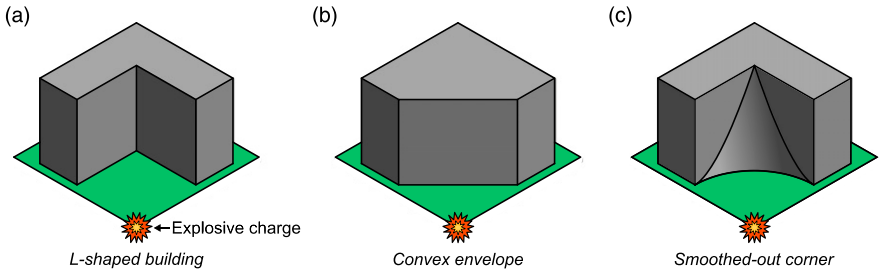

Figure 8. Schematic drawings of the three building shapes numerically investigated by Gebbeken and Döge (2010) comprising (a–b) two common shapes and (c) a non-convex design which reduced the blast loading.

et al., 2020) have highlighted the need to consider the complexities of cityscapes and their influence on blast loading in urban environments. The following paragraphs describe aspects of cityscapes that have been probed by researchers over the last few decades.

Smith and Rose (2006) experimentally measured the pressures along different street configurations: straight, cul-de-sac, 2, 3 and 4 street intersections. The cul-de-sac was found to have the maximal pressure amplification amongst the various combinations that were tested. They also found that for each configuration, the volume available for the blast wave to expand may be used as a metric to evaluate the attenuation characteristics. Another interesting finding was that the pressure amplification down a street lined by buildings was found to depend on the height of the buildings and the street width, viz., wider streets and shorter buildings would minimize amplification. For these purposes, a scaled street width of 4.8 m/kg$^{1/3}$ and scaled building height of 3.2 m/kg$^{1/3}$ were experimentally found to be as good as infinite extents for minimizing and maximizing the blast amplifications, respectively. It was also observed that the distance of the charge from the junction influences the extent to which the blast diffracts, and enters the other streets leading off the junction. The larger the distance of the charge from the junction, the greater the degree of diffraction that occurs at the junction, as opposed to the reflection and transmission down the street in which the charge is located.

Fouchier et al. (2017) report a 1:200 scale table-top experiment to carry out an in-depth study on the effect of street junctions and channelling in an urban environment. The conclusions from this study are broadly similar to those reported earlier by Smith and Rose (2006) – that overpressure enhances downstream of a narrow street as the incident wave coalesces with that from reflection off the walls of the street. They explored the effect of a 136 mg TNT equivalent explosion using an RP80 detonator on a building configuration shown in Figure 11. Paradoxically, channelling (confinement) was shown to have a beneficial effect here as the pressure and impulse values recorded amidst the buildings were similar to the free-field scenario. This could be because the buildings were not tall enough to be considered as confined (i.e. scaled building height < 3.2 m/kg$^{1/3}$). At the exit point of this building complex (shown in Figure 11), the pressure was reduced by up to 80%. The authors further noted based on their experiments that straight streets were deemed to be the more destructive street configuration, whereas a four-way intersection was found to be the least destructive.

Conditions typical of streets in European cities (6–20 m wide and 20 m tall buildings) and explosions ranging from 100 to 10,000 kg to include truck bombs were considered by Codina et al. (2013). Two different scenarios of an explosion were simulated, one initiated at the centre and the other one off-centre, so as to recreate an explosion initiated on the pavement at 2.2 m distance from the building. They report that channelling (confinement, leading to coalescence of waves) is a

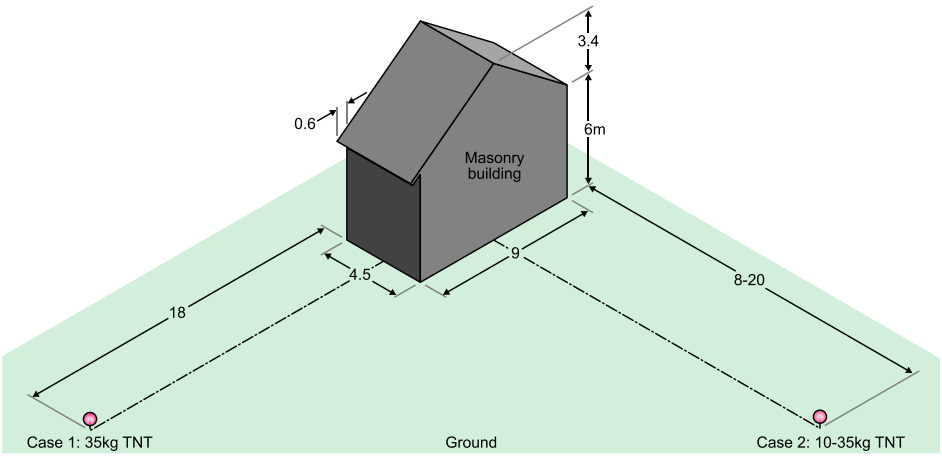

Figure 9. A schematic representation of the two test cases investigated by Xiao et al. (2021) to experimentally determine the pressure evolution on a gable roof building subjected to different explosive loadings.

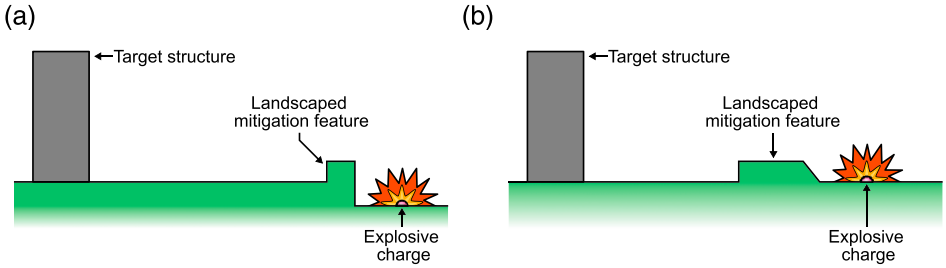

Figure 10. A representation of landscaping techniques that may be used to improve blast mitigation (Barakat and Hetherington, 1999).

serious effect as increases in overpressure of up to 8 times were observed. Expanding on the previously reported research, they provide a broader reason for the pressure amplification in confined spaces based on their identification of four zones – Unconfined Area, the Regular Reflection Area, the Mach Reflection Area and the Confined Area (Figure 12(a)). But unlike the overpressure, for impulse, the increase is attributed to the confinement itself and not due to the interaction amongst the multiple waves. The confined area occurs at 1.65×width, irrespective of the TNT charge mass, suggesting that a street wider than 30 m (1.4 – 6.5 m/kg$^{1/3}$) will lead to an absence of confinement. This is quite different from the 4.8 m/kg$^{1/3}$ value that was proposed earlier (Smith and Rose, 2006) and the reasons for this discrepancy are not fully clear. A similar identification of zones was also undertaken for the case of an asymmetric explosion (Figure 12(b)). While the classification of zones was unchanged, their locations were slightly different.

Research on the role of frangible façades on buildings along a street revealed two contrasting aspects (Smith et al., 2003). Frangible façades can minimize the pressure amplification down the street. But then, the amplified overpressures inside the building would be high enough to cause harm to the occupants of the building. So they recommend the use of façades robust enough to withstand

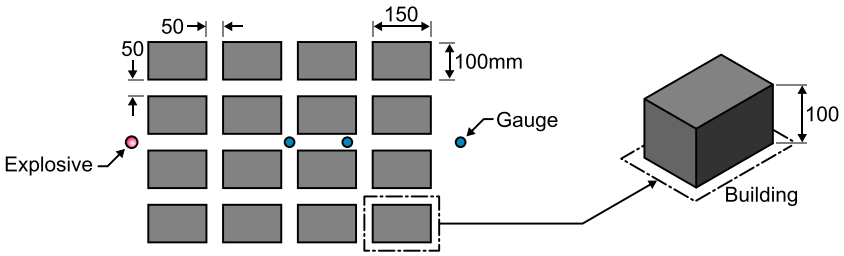

Figure 11. A schematic of the test setup used by Fouchier et al. (2017) to investigate the effect of blast wave channelling between densely spaced buildings.

an explosion in the mid- to far-field, but not near-field. Parenthetically, mention is made of some studies where the role of an opening on a structure may be taken to simulate a broken window. The effect of such 'pre-formed openings' on the failure mode is available for a metal wall (Aune et al., 2017) and a concrete wall (Mays et al., 1999).

With regard to a cluster of buildings, it was consistently observed that the interaction of a blast with the first row of buildings was the dominant factor in defining the extent of shielding offered to the subsequent rows of buildings. The effects of channelling and attenuation that may be produced by buildings in a residential layout were explored for a 1:34 scale representation of two storey 'semi-detached' buildings (Smith et al., 2004). A scaled down 25 g TNT equivalent charge was placed within a residential zone, each having different areal ratios, defined as the ratio of the footprint of the building area to the total area available. Air3D simulations were then validated against this data and then used for subsequent analyses. An average reduction in loading of only 10% was observed for areal ratios ranging from 17.9% to 28.6%. The final loading, as the authors report, is a complex combination that depends on both the channelling and the shielding effect produced by neighbouring buildings. The more congested buildings (higher areal ratio) had a lower reduction in pressure, suggesting that channelling is more dominant than shielding. They suggest that complete numerical simulations for each scenario are required to understand the loading evolution in such conditions. In a related but different set of simulations on buildings, Remennikov and Rose (2005) show how a building in the shadow region of another shorter building can be shielded and thus experience reduced loads. The asymptotic limits on the street width that were mentioned earlier (Smith and Rose, 2006) were also validated in this work.

To evaluate the overpressure loads arising on a building due to an explosion in the street, an engineering method (Von Rosen et al., 2004) to superpose the loads is available. This was adapted by Johansson et al. (2007) for buildings at an intersection (Figure 13(a)) using a combination of incident pressure values and diffraction coefficients. The resultant plots were compared with AUTODYN data that had been validated against a $1/5^{th}$ scale experiment. Fairly good correspondence (given the minimal computational effort) was obtained, as shown in Figure 13(b). This validation was for the overpressure range of 50–100 kPa.

General outlook on direct loading

The role of clearing in reducing the overpressure on objects with straight faces was explored and several empirical approaches to estimating the loading on W-sections, cuboids, flat face of a cylinder and parallelepipeds were presented. The addition of curvature to finite-sized objects causes a further reduction in pressures due to the relieving effect introduced by the (concave) curvatures. Empirical

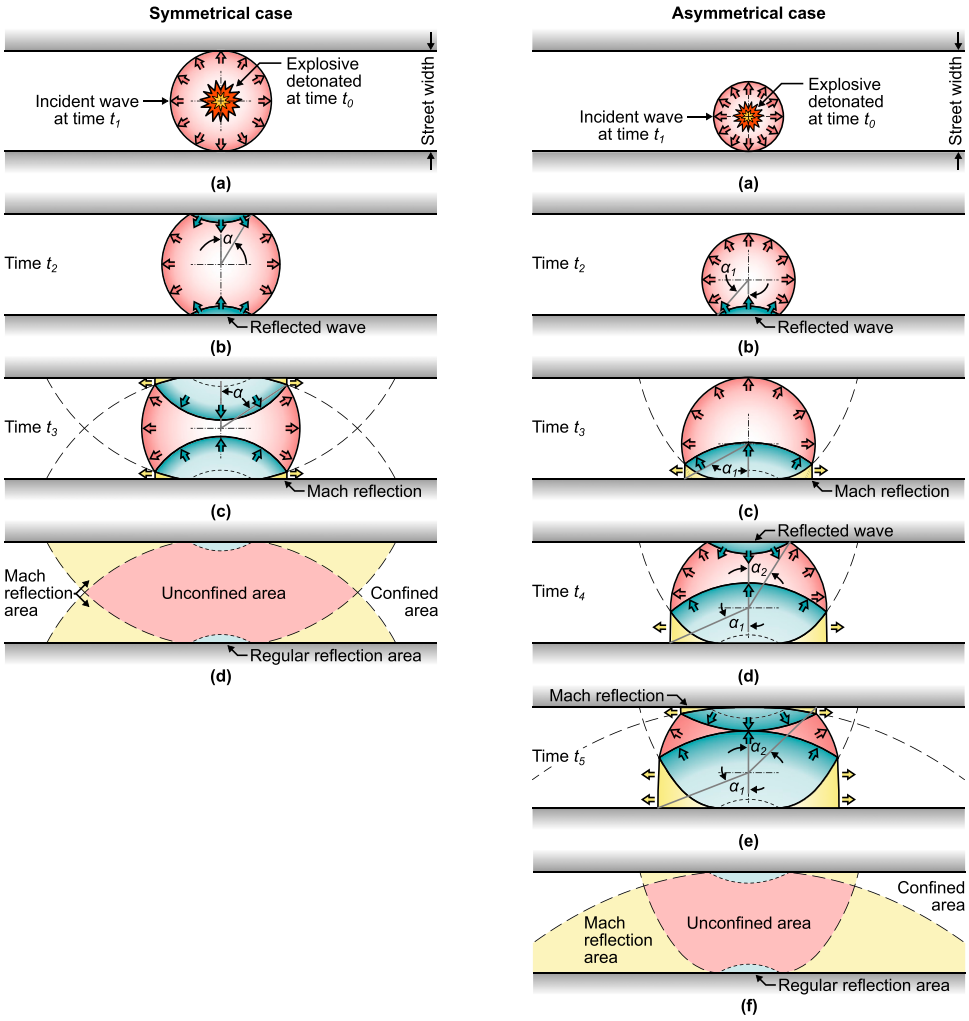

Figure 12. A schematic representation of the propagation of waves resulting from an explosive detonated at time t_0 in a street layout for (left) a symmetrically located charge and (right) an asymmetrical one (Codina et al., 2013).

models are available for a full cylinder, curved face of a hemi-cylinder and hemispherical structures with a cylindrical neck. While these are applicable to individual buildings, for structures in an urban setting, the effect of street width and height of buildings in confining a street explosion have been documented using experiments at different scaling ratios, with 1:200 and 1:10 scale experiments, all reaching similar findings. The role of different junctions – straight, cul-de-sac, 2, 3 and 4 street intersections – in modifying the intensity of an explosion have also been studied, although the length down the street for which a blast wave may be considered to have weakened considerably has not been clearly documented yet.

Having presented aspects of direct blast wave loading on target structures of various shapes, we next move on to indirect loading cases, where the properties of the blast wave are modified by

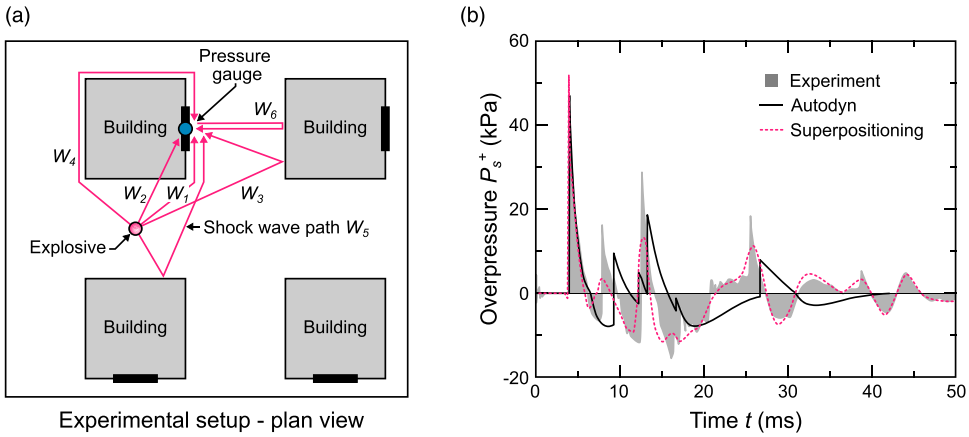

Figure 13. (a) A schematic plan view of the test setup used by Johansson et al. (2007) to investigate the effect of corners on blast load estimation. The experimental results are shown in (b) alongside the response numerically predicted by Autodyn and the estimation based on the superpositioning method (Von Rosen et al., 2004) calculated by combining the diffraction coefficients for the shock wave paths W_i.

another structure *before* it impacts the structure of interest. In other words, here we consider the evolution of a blast wave *downstream* of an obstacle on, rather than on itself.

Indirect loading: Barriers

Introduction

A barrier is defined here as a wide blockade in the path of the blast wave that results in a strong reflection wave (Figure 14) directing energy away from the protected structure. Further, due to the presence of a barrier, a diffracted wave arises from each free edge of the barrier, and these diffracted waves further weaken the transmitted wave. In this context, research on the effect of the height of the barrier, the distance behind the barrier where shielding occurs and the role of a canopy placed over this edge have been undertaken (Beyer, 1986; Xiao et al., 2019). The thickness of the wall (Sha et al., 2014), referring to the breadth in Figure 15; the detrimental effect of increasing height of burst (HoB) (Chapman et al., 1995b); the inclination of the face of the barriers (Sugiyama et al., 2015); the structural integrity of the wall (Rose et al., 1998) and even a not so obvious aspect such as the roughness of the barrier (Hajek et al., 2016) all play a role in weakening the wave transmitted beyond the barrier. Moreover, if the length of the barrier is short, waves diffracted from either end propagate towards the centre line of the shadow region of the barrier and can cause pressure amplification under certain conditions. The extent to which these parameters affect the strength of the transmitted wave has been an ongoing topic of research (Beyer, 1986; Chapman et al., 1995b; Rose et al., 1995, 1997) and a brief summary of these aspects is provided in this section.

Clearly, the protection offered by a barrier depends on the dimensions, especially, the height of the barrier. To this end, Beyer (1986) conducted 1:6 scale experiments using different masses of C4 placed near an armour steel wall, with Z_{TNT} ranging from 0.18 to 0.44 m/kg$^{1/3}$. The charge was centrally located at a height of 0.3 m above the ground and 0.3 m in front of the barrier. The authors reported attenuated pressure values behind the barrier, in the form of tables and charts, along a line drawn from the charge and:

- perpendicular to the wall (1*H*–8*H*),
- at 45° to the barrier (2*H*–8*H*) and
- at points at a height *H* directly above the previous locations (2*H* for the last one in the array).

The extent of attenuation reduced with increasing distance away from the barrier, as shown in a typical pressure plot in Figure 15(b), but for most tests reported, this protected region extended all the way up to 8*H* behind the barrier.

Covering a broader region behind the wall, a similar set of experiments (Z_{TNT} = 0.17 m/kg$^{1/3}$) were reported by Rose et al. (1995). This was for a 1:10 scale experiment using 75 g TNT equivalent mass at a distance of 0.138 m from the wall and 0.109 m above ground. The wall was a steel structure 0.35 m tall (*H*) and 2.1 m long. Pressure measurements up to a height of 3*H* and until a length of 6*H* were carried out behind the barrier, on a plane perpendicular to the barrier and the ground, passing through the mid-point of the barrier. Except for a small region above and behind the wall where the effects of the reflected wave persisted, substantial pressure and (slightly lower) impulse attenuation were observed at all measurement locations. Broadening the scope of the experimental campaign to include scales ranging from 1:8 to 1:14, pressure and impulse charts behind barriers of different scaled heights were later reported in Rose et al. (1997). The combined dataset behind the barrier from both studies covered a wide range of scaled distances from 0.5 to 4 m/kg$^{1/3}$ and from 0 to 2 m/kg$^{1/3}$ above the ground. The scaled heights of the wall ranged from 0.5 to 1.0 m/kg$^{1/3}$.

Chapman et al. (1995b) performed experiments at 1:10 scale, with $Z_{B,TNT}$ = 0.38–3.5 m/kg$^{1/3}$ to the wall. They used a barrier that was H_B = 300 mm tall, with TNT charge masses ranging from 40 g to 80 g, placed at HoBs from 0.05 to 0.3 m. Pressure was measured at different heights (H_T=0.5*H*–2*H*) along the centreline of a target structure placed at a distance (d_T=0.15–0.6 m) behind the barrier. An empirical relationship was also developed to obtain the pressure and impulse values on the wall (cf., sub-section on *Indirect Loading*).

In the aforementioned studies, the depth of the walls was small enough for their thickness to *not* influence the properties of the blast wave. Zhou and Hao (2008) numerically studied an infinitely

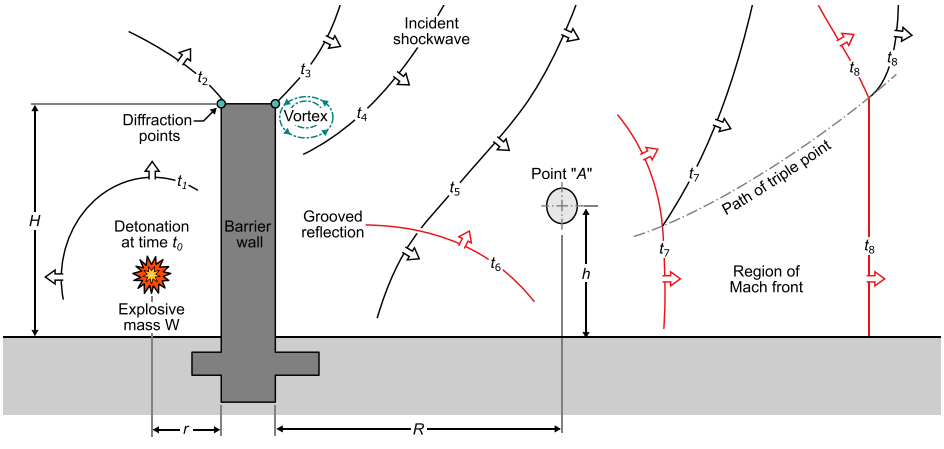

Figure 14. A schematic illustrating the complex shock wave development arising from an explosive detonated at time t_0 that interacts with a barrier wall. The effect of the two diffraction points on the path of the incident shock wave is evident. Figure adapted from Beyer (Beyer, 1986).

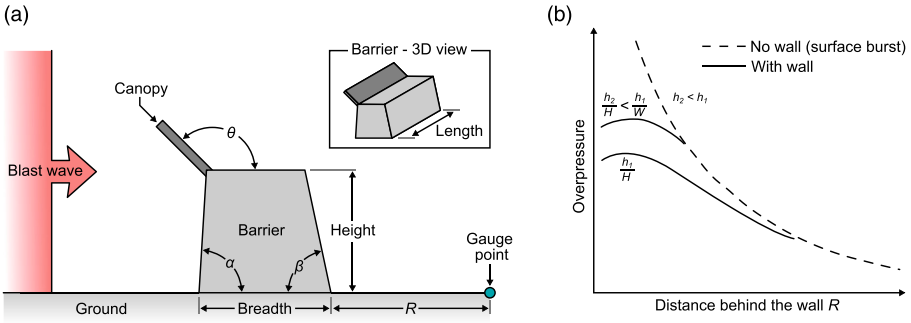

Figure 15. (a) A schematic diagram detailing the barrier nomenclature used in this paper. (b) A graph illustrating the peak pressure distribution as a function of distance behind a barrier wall contrasted with a no wall (surface burst) case (Beyer, 1986).

long blast wall of 250 mm thickness (as varying thickness from 150 to 300 mm showed insignificant difference in loading), varying the mass of explosive from 10 to 10,000 kg of TNT. The height of the barrier was varied from 1 to 4 m, the height of the building varied from 3 to 40 m, the distance from charge to building varied from 5 to 50 m (barrier location was set between 0.2 and 0.8 of this value, i.e. 1–40 m) and the HoB was fixed at 0 m. Based on these results, empirical formulae were developed for prediction of peak pressure, peak impulse, arrival time and decay time, on a building behind the barrier. It was noted that there exists a location along the height of the building where maximum reduction in pressure and impulse may be observed. This was then correlated to the input conditions. Using these findings, a linear piece-wise function was developed for predicting the variation of pressure over the face of the building.

The role of barrier dimensions

Payne et al. (2016) carried out a parametric study using CFD to determine regions in the wake of a cuboid shaped obstacle (3.50 × 3.95 × 3.00 m) where the overpressure and impulse values were *unaffected* by the presence of the obstacle, that is, where incident blast conditions were restored. It was found that the pressure field behind the obstacle is reduced only in the near-field, with the mid and far-field largely unaffected. Conversely, impulse values were significantly reduced even until the mid-field, while also increasing slightly in certain regions due to complex wave interactions, and eventually returning to incident conditions in the far-field. The authors provided a table showing distances beyond which free-field incident impulses recover. The converse of this finding being that within this region, some attenuation is generally observed, which is the focus of this article. As a rule-of-thumb, the shadow region behind the target was seen to extend to a maximum of 60° from the rear corner. The TNT charge mass was fixed at 100 kg and the stand-off distances were varied from 15 to 50 m in steps of 5 m.

A parametric study to understand the role played by each dimension of a barrier was reported by Miura et al. (2013) for a TNT equivalent explosive mass of 3400 kg. Numerical simulations were carried out for blast propagation over a structure that may be considered to be a barrier with finite dimensions. Its dimensions were varied with the intention of studying the potential mitigation effects of dikes that surround energetic material storage sites. For the narrowest length that was simulated (1.17 m/kg$^{1/3}$, from the range of 1.17–7.71 m/kg$^{1/3}$), overpressures on the ground were found to be higher downstream of the wall, although all the other simulated lengths resulted in a

pressure reduction in the downstream. This was attributed to the interaction of the diffracted wave from the edges of the barrier, with the wave reflecting off the ground surface behind the barrier. For long enough lengths, the differences were negligible, and so 2D axisymmetric simulations were subsequently used for a parametric study of the dimensions. This was because the 2D simulations gave similar pressure histories as the 3D simulations but at a significantly lower computational cost. The investigated parameters were scaled heights of barrier: 0.13–0.8 m/kg$^{1/3}$, scaled distance to front face of barrier: 2–4.3 m/kg$^{1/3}$ and scaled width of barrier: 0.067–1.064 m/kg$^{1/3}$. The height of the dike was identified as the most significant parameter in influencing attenuation, but since constructing a tall barrier is not always practical, the effect of stand-off to the dike and the dike width were also explored. The most significant attenuation was obtained for the maximum dike height and minimum scaled distance, as the diffraction angle of the wave at the dike edges would then be the highest. For the cases where the dike was far from the blast source, unlike the other stand-off scenarios, the breadth played a minimal role. This was thus approximately simulated by using an infinitely thick barrier (or a back-step), and a correlation for the maximum pressure behind the dike and an empirical 'effective thickness' of dike was provided.

A preliminary numerical and experimental study, using 0.5 g of PETN (stand-off distance of 40 mm) explored the role of two small dikes (Sugiyama et al., 2015). The first: a flat faced obstacle, with a flat top and a sloping rear face ($\beta < 90°$), and the second: an inclined front face ($\alpha < 90°$), a flat top and a sloping rear face ($\beta < 90°$). While the effects of the dike on the flow field were found to be non-existent in the far-field, in the near-field, the obstacle with the flat face performed marginally better. Intensification of the blast wave in the intermediate downstream regions was reported, and this was attributed to complex wave interactions.

Numerical experiments on a shock tube were carried out to study the effect of barrier geometry on an incident shock wave by Sha et al. (2014) using an incident shock overpressure of 300 kPa. Not including structural strength considerations, the breadth of a barrier element was found to amplify the interaction between the reflected wave and the incident wave. So the breadth ought to be as narrow as possible to achieve the best attenuation. Adding a positive slope ($\alpha > 90°$) on the windward side gave an improved attenuation (Figure 16). Incidentally, as described later, Berger et al. (2015) in a slightly different context have experimentally validated this concept. On the other hand, the effect of the slope on the rear face was found to be comparatively small. Zhou and Hao (2008) had also reported an insensitivity to barrier thickness; this may also be due to the insignificant values of scaled thickness of the barrier. But for blast pressure downstream and not far off from a dikes (Miura et al., 2013), the width was shown to modify the pressure values. This could perhaps be attributed to the use of a planar wave in the work of Sha et al., where the incidence angle between the shock and the barrier is always the same, unlike in the work of Miura et al. (2013), where the blast wave was curved and not planar.

The role of a canopy

The role of a metal canopy (Figure 15) was first explored by Beyer (1986), and the details of the experiment may be found in the previous sub-section and also in Table 2. Three canopies (first: 21 kg/m^2, 3 m long, 0.3 m wide; second: 40 kg/m^2, 3 m long, 0.3 m wide and third: 40 kg/m^2, 3 m long, 0.45 m wide) were tested. In general, they were all found to provide improved mitigation than the reference (no canopy) case. Between the canopies, no clear trend could be determined, but the lighter one performed slightly better in terms of impulse, and the heavier one performed better in terms of overpressure.

Recently, Xiao et al. (2019) extended this work to understand the role of the canopy angle. Experiments were carried out using a 3.9 kg PETN charge, placed at the centre of a 10 m diameter circle (on plan), 0.4 m above ground level. Three types of gabion walls were placed equidistantly along the perimeter of the circle (Z_{TNT} = 2.92 m/kg$^{1/3}$): one was fitted with a forward inclined metal canopy, one with a rear inclined canopy and one was left without a canopy. The barriers measured 2.0 × 1.0 × 2.0 m, and the canopies were 0.75 m long, with inclination angles (θ, Figure 15) of 135° and 45°, respectively. Reflected pressure measurements were made at distances of 10 m from the charge, and 5 m from each gabion wall barrier. Since the breadth of each gabion was not sufficient to prevent the sideward ingress of the diffracted blast wave, a series of numerical simulations (initially validated against these experiments) were then used to compute the flow evolution for an infinite-breadth wall to avoid this sideward ingress. The results showed that the addition of canopies improved the blast attenuation performance and the forward inclined (θ =135°) canopy gave the best attenuation. The optimal values for the inclination of the canopy were in a narrow band around θ =115°. As described earlier, using a shock tube, Sha et al. (2014) had also reported that a forward inclined obstacle[8] produced improved attenuation. Contrary to this finding, Hajek et al. (2016) report that the overpressure values behind a barrier are almost insensitive to the forward facing angles of canopies, possibly due to the charge (0.5 kg) being detonated closer to the barrier (0.75–5 m, Z_{TNT} = 0.9–6.3 m/kg$^{1/3}$). This, it may be noted, adds credence to the earlier comment on the (non)-planarity of the wave altering the physics of the interaction.

Additional barrier parameters

Experiments on frangible walls were reported by Rose et al. (1998) using 75 g of TNT equivalent charge placed close to the barrier; conditions similar to their earlier work (Rose et al., 1995). In this work, 'walls' of water, sand and ice were shown to perform better than a steel wall, both in terms of overpressure and impulse attenuation. Experiments using walls of other materials, such as geo-textiles and plastics, were also undertaken. All materials, including material such as thin balsa wood (< 2 mm) and even polythene sheet (< 1 mm) gave a reduction in overpressure (but not impulse) as compared to a no wall case. They concluded that so long as a wall stays in place to cause the wave to diffract around it, either by means of its inertial mass or due to the shape of a resistant structure, the system can mitigate a blast wave.

While frangible walls can cause harm to people in the surroundings due to fragmentation, the use of water-filled 'walls' can avoid such a scenario. This shows how barriers can mitigate a blast wave by reflection, diffraction or even absorption of energy (Xiao et al., 2019). A summary of these and related work in the recent period, and details on the construction of barriers may be found in the

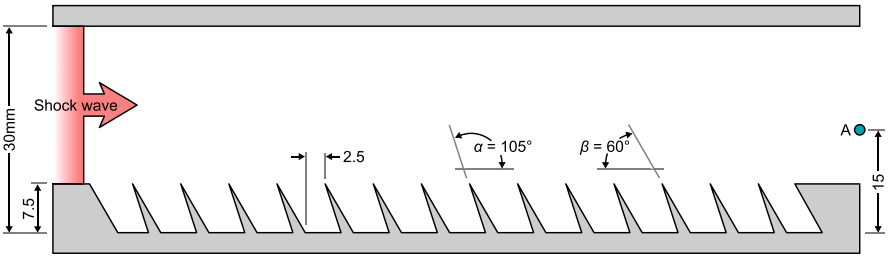

Figure 16. The shape of an optimized barrier for maximal attenuation downstream (at location **A**) reported by Sha et al. (Sha et al., 2014) using 2D numerical simulations.

Table 2. Summary of literature on barriers and blast wave interaction.

Barrier type	Representative scale	TNT Eq. weight (or incident pressure)	Stand-off distance (or decay time)	Loading estimates
Metal wall with canopy	0.68 × 8.6 m, canopy 0.3,0.45 m	0.5, 4, 7.6 kg	0.3	Tabulation (Beyer, 1986)
Metal wall	0.35 × 2.1 m	0.075 kg PE4	0.138	Tabulation (Rose et al., 1995)
Metal wall	0.35 × 2.1 m	0.075 kg PE4	0.138	Extension (Rose et al., 1997) of Rose et al. (1995)
Metal wall	0.3 × 2.1 m	0.04–0.08 kg TNT	0.15–1.2 *m*	Empirical formula (Chapman et al., 1995b)
Wall	L:Infinite, B:300 mm, H:1–4 m	10–10000 kg TNT	1–40 m	Empirical formula (Zhou and Hao, 2008)
Finite barrier	3.50 × 3.95 *m* × 3.00 m	100 kg	15–50 m	Tabulation (Payne et al., 2016)
Frangible walls	0.3 × 1.5 m (approx.)	75 *g* (*eq. TNT*)	138 *mm*	Plots (Rose et al., 1998)
Finite barrier (Dike)	B: 1.95–12 m, H: 1–15.96 m	3400 *kg* (*eq. TNT*)	30–64.5 m	Empirical formula (Miura et al., 2013)

review by Smith (2010). The effect of contact charges, which are used to pulverize the barriers, was studied by Coughlin et al. (2010). Such studies involve considering energy absorption by the material of the barrier, which is beyond the scope of this review. Additional details on such research may be found in the work of Zong et al. (2017).

The role of roughness on the face of a barrier has also been shown to introduce disruption to the flow and attenuate blast pressures (Hajek et al., 2016). Pyramid shaped corrugations made of concrete and acoustic foam panels were attached to the face of a concrete barrier and attenuations were found to increase behind the barrier for $Z \sim 1.5$–10 m/kg$^{1/3}$. Incidentally, the acoustic foam material performed better than the bare concrete elements for reasons that were not immediately clear, but it proves the hypothesis that roughness plays a role in reducing the attenuation. Such an attenuation was also reported by Makki (2017) for shock loading experiments on rough metal plates using a shock tube. A zigzag shape (plan view) of a sand wall (Rose et al., 1998) was also shown to result in an improved performance (measured at $Z = 3.5$–4.2 m/kg$^{1/3}$). All these suggest that roughness on the surface of barriers can indeed enhance attenuation.

To understand the effect of stacking several barriers, Benselama et al. (2010) experimentally studied blast propagation over a series of three barriers. Barriers of dimensions 8.5 × 0.6 × 0.6 m, spaced 1.2 m apart (in the direction of blast propagation) were used in this experiment. A 416 g TNT equivalent mass was detonated at a distance of 1.7 m from the first barrier and they found that blast pressure attenuation is effective only beyond the second barrier. They also reported that height-to-spacing-between-barriers ratio played a more important role than the breadth-to-spacing-between-barriers ratio.

While the use of barriers is more common outdoors, Santos et al. (2018) discuss the role of a 'meandering wall' placed ahead of an access control zone inside a building. This could be helpful, in spaces such as in a hotel lobby, to mitigate the effect of an explosion from a luggage bomb. They report a reduction in peak overpressure and impulse values in the protected region, based on a

numerical experiment conducted using 25 kg TNT at a distance of 3–5 m from the rigid wall. This shows the potential use of having barriers even inside buildings under special conditions.

General outlook on indirect loading: Barriers

A reduction in overpressure values was found for distances of up to 8 times the height of a blast wall. Experiments on frangible walls showed attenuated pressure values downstream. This suggests that the strength of the wall is not the primary contributor to attenuation, but instead, it is shock diffraction that plays a dominant role. While it is intuitive to understand the prominent role played by the height of the barrier, the importance of having a long wall to avoid hotspots of overpressure behind the wall and the relatively low importance of thickness of the barrier to enhance attenuation have been key findings of research on this topic. Empirical formulae to obtain the pressure on a plane target wall behind a barrier are available for a wide range of parameters. A forward inclined canopy, and a rough surface for the barrier, were both found to enhance attenuation. It is worth noting at this point that the role of target clearing has not explicitly been considered thus far in any of these studies, as the focus was on explosions located relatively close to the barrier.

In an urban environment, blast protective structures (e.g. blast walls and other obstacles) should be unobtrusive and, ideally, blend in with the surroundings. A number of suggestions have been provided in FEMA (2007) guidelines. While the research on barriers and canopies has shown an appreciable increase in protection in the immediate shadow region, the use of these barriers in a cityscape may not be appropriate as they give the unwanted appearance of a garrison. The additional risk of fragmentation is also an important consideration, and so barriers do not easily go with an urban landscape (Zong et al., 2017).

Researchers thus began exploring the possibility of using small barriers and posts, such as bollards, which are part of any urban streetscape, to mitigate a blast wave. Can smaller obstacles and a transition from an absorption-type to a deflection-type blast attenuation technique still return similar levels of protection? This forms the topic of the next section, namely, the use of obstacles, rather than barriers, to achieve mitigation.

Indirect loading: Obstacles

The interaction of a blast wave with a structure is characterized by several complex flow features, such as reflection, diffraction, vortices and the various interactions within these features. Bazhenova et al. (1984) describe how the study of shock wave motion over simple objects – for example, a case of reflection off a concave corner or a diffraction off a convex corner along the direction of propagation of a shock wave – can be used to understand flow patterns over more complex structures. In the following sections, we first address relevant research on simple obstacles and then progress on to groups of obstacles.

Single obstacle

Typically, previous studies on obstacles involved a flat-top pressure profile – generated by a shock tube – than the decaying pressure profile that is characteristic of blast waves. Since these loads have a steady pressure for at least a few milliseconds after the instantaneous shock pressure jump, the decay time of these waves is not clearly defined. Thus, most descriptions of the strength of the wave are in terms of the Mach number. Typically, they are in the range of 1.2–1.8, whose scaled stand-off distances would then be between 2 and 3.5 $m/kg^{1/3}$ for a surface blast.

Analytical predictions for the shape of the diffracted wave were given by Whitham (1957). To validate this method, high Mach number (M_s = 3) shock tube experiments on the flow involving steady, strong shocks over cones, a cylinder and a sphere were carried out (Bryson and Gross 1961). It was then shown how the flow field may be reconstructed for a particular obstacle shape using numerical integration of the appropriate flow equations or by using the method of characteristics. Interestingly, the authors found that the diffraction pattern was independent of the Reynolds number, and it is suggested that this is likely to also be true for blast waves since they are both impulsive flows.

The role of a circular pole (~64 mm diameter) in disturbing the flow field was studied using CFD (Christiansen and Bogosian, 2012). For a single pole placed between the target and explosive, overpressure and impulse reduction were achieved on the target for stand-off distances between 0.52 and 0.72 m/kg$^{1/3}$. Using three poles (one ~64 mm and two ~ 50 mm diameter) in a triangular arrangement, with the bigger pole facing the explosion and the smaller ones behind it, the reduction in overpressure and impulse was enhanced twofold. Dey et al. (2020) used ANSYS Fluent to study the pressure field around generic obstacles: sphere; cone; and cylinder, all having equal frontal dimension and overall length. They found that the strongest initial wave reflection was seen for the cylinder, followed by the sphere and then the cone. The re-attachment of the shock behind each of these objects was found to be the quickest for the sphere, then the cylinder and finally the cone.

Hahn et al. (2020) performed CFD simulations in order to study the pressure and impulse field that evolved on a façade behind a cylinder at high Mach numbers, which corresponds to scaled distances of $Z \sim 0.4$–1.5 m/kg$^{1/3}$. The authors noted the presence of a pressure increase behind the column, even up to a distance of 12D, excluding a very narrow region of 0.5D behind the pole, where the values were 15%–20% lower than the corresponding free-field value. A subsequent increase in impulse, to almost double the incident value, was observed behind the column, occupying a narrow band extending approximately 45° behind the pole. The high pressure immediately behind the pole arises because the pressure wave wraps around the circular cross-section of the column and re-forms, leading to multiple reflections. For a specific case ($Z \sim 0.6$ m/kg$^{1/3}$, D = 0.3 m), where a façade was located 1 m behind the cylinder, a 14% increase in pressure was observed. The column height effects were not considered, as analyses were performed in 2D.

Multiple obstacles

State-of-the-art. Dosanjh (1956) studied the transmission of a shock wave through a wire grid and showed that the flow is influenced by the choked area of the grid. This is because area reduction, as expected, inhibits the flow. This finding has since been confirmed repeatedly by several researchers, all of whom showed that the area ratio controls the flow downstream of an array of obstacles (Monti, 1970; Honghui and Yamamura, 2004; Epstein and Kudryavtsev, 2012).

Honghui and Yamamura (2004) studied the passage of a shock wave (M_s = 1.4–1.9) through spheres and cylinders arranged as rows of ball and stick (3 and 4 mm diameter) models. They observed a direct correspondence between the attenuation and the blockage introduced by each model. Increasing the spacing between rows beyond 15 mm did not influence attenuation in the case of smaller spheres (10 mm) diameter, but for the larger spheres (20 mm diameter), it proved beneficial. It is to be noted that for the larger sphere experiments, the maximum spacing inspected was up to 30 mm. The authors also reported increased attenuation with more rows and also with stronger shocks (higher Mach number).

Britan et al. (2006) investigated shock transmission through porous barriers (porosity: 0.15–0.7) of different geometries for M_s ranging from 1.35 to 1.7. They concluded that the porosity and not

geometric factors (including shape, thickness and hydraulic diameter of the opening) determined the level of attenuation. Increasing the distance between the end wall and the barrier caused a linear reduction in overpressure, and for distances beyond 50 hydraulic diameters, viscosity began to play a role.

Sasoh et al. (1998) investigated the effects of pseudo-perforated walls on very weak shock waves (M_s = 1.02–1.12) travelling in ducts, building on previous work and showed that, unlike weak shocks, it takes relatively shorter lengths to attenuate a Mach 1.5 shock wave (Craig 1977). They found that the length of the pseudo-perforated wall section is an essential parameter and should be increased to achieve better attenuation. This concept has implications on the roughness of elements implemented for blast attenuation studies, and is also well corroborated by earlier work on roughness of a barrier surface.

A flap valve is a dynamic barrier whose orientation depends on the shock strength (Figure 17). Investigating the potential benefits of a flap valve for Mach numbers 1.2 and 1.4, Berger et al. (2015) report that for the same porosity ratio, a barrier inclined at α=135° (upstream) to the flow showed 15% higher attenuation than the one at 45° (downstream). As an aside, the overpressure data for these angles are similar to the findings of Xiao et al. (2019) for a canopy on a barrier wall.

Chaudhuri et al. (2013) studied the transmission of shock wave (M_s = 1.4) through 4 rows of obstacles with the following shapes:

- triangle (vertex pointing upstream),
- triangle (vertex pointing downstream),
- square,
- circle.

2D numerical simulations showed that the backward facing triangle (a divergent opening) was the most effective in attenuating a shock wave. This was also confirmed by Prasanna Kumar et al. (2018) for a higher incident Mach number of around 2.7. This finding shows that at low porosities (~0.25), the geometry of the obstacle also plays a role in the attenuation. However, for the upstream side of the obstacle, that is, the reflected shock wave, they observed that the wave is attenuated when the obstacles have a converging shape (upstream facing triangle). In what is essentially a combination of these two concepts, Skews et al. (1998) reported the concept of shock trapping to enhance the mitigation of a shock wave. This concept was further validated in the work by Seeraj and Skews (2009).

A logarithmic spiral is a well-known arrangement used to focus shock waves. Instead of placing obstacles along straight rows perpendicular to the flow direction, Wan and Eliasson (2015) extended these M_s=1.4 simulations further to study the effect of placing them along a (longer) logarithmic spiral. This contrivance has a lower porosity value and could thereby improve the attenuation performance. While it provided good attenuation at the spiral's design Mach number, an enhanced attenuation performance was observed for a stronger than design incident shock (M_s = 1.5). However, the logarithmic spiral generally under-performed for lower Mach numbers. Surprisingly, the pressure upstream of these obstacles did not increase in a manner commensurate with the higher blockage ratio that should have led to a stronger reflection. This implies that the use of a logarithmic spiral can be explored for situations where protection is desired along both sides of the barrier.

Niollet et al. (2015) used 20–70 g PE4 in a blast tube to study the mitigating effect of an arrangement of cylindrical poles ahead of a target structure (a metal plate). They found that the target experiences either amplification or amelioration of the blast load, depending on the arrangement of the bars. A staggered arrangement of the cylinders was shown to be more beneficial towards

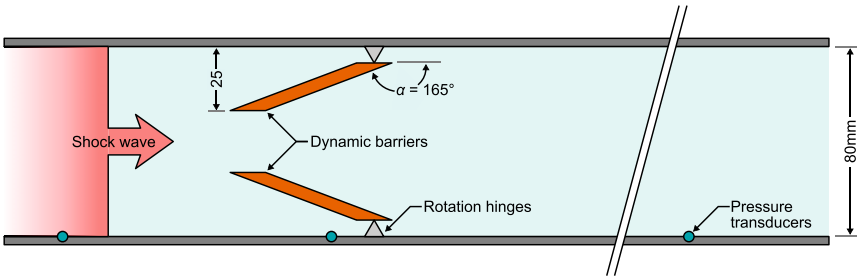

Figure 17. A schematic representation of the dynamic barrier concept as reported by Berger et al. (2015), comprising of a pair of hinged barriers inclined towards the incident shock wave.

amelioration. They also noted that placing the bars too close to the test plate would cause more damage as the reflected wave gets trapped, leading to an increased loading duration. The impulse of these tests ranged from approximately 40 to 100 N.s over an exposed area of 200 × 200 mm.

The role of surface roughness was experimentally and numerically explored by Ivanov et al. (2019) for $M_s = 1.2$ by using obstacles (10 × 10 mm) with and without small undulations (dimples of $R = 0.58$ mm) on its surface. Despite observing additional vorticity in the downstream of the flow due to these serrations, they did not detect any significant difference in the attenuation values. This was attributed to the small sizes used for the simulations, whose disturbances were perhaps not sufficient to give rise to a marked improvement in attenuation. This should be contrasted against the results reported in the previous section, where the surface roughness played a significant role in attenuation.

For further reports on studies over obstacles, one may refer to the detailed review by Igra et al. (2013) and a summary of the literature in Wan and Eliasson (2015).

Special case: Rigid porous media. A very special case of the multiple obstacle scenario is the interaction of a shock wave with porous media. The resultant transmitted pressure is (usually) not instantaneous, providing additional time for the structure to be loaded fully, which can result in the target structure experiencing a less severe, non-impulsive load. Ram and Sadot (2013) describe an elegant semi-analytical method to estimate such overpressure loads on the end wall of a shock tube, located at a distance L from the rear face of a slab of porous media. Due to the presence of voids in the porous barrier, the effective (open) length from the rear face of the porous barrier would now be longer, L_{eff}. This zone may be considered to be a confined zone filled with ambient air having specific heat ratio, γ. As the blast wave travels across the barrier and transmits to the other side, it may be taken to be the equivalent of pressurizing this confined zone from the upstream side of the porous barrier following an isentropic process. From this, a simple equation (equation (4)) for the evolution of pressure was then proposed and experimentally validated using a shock tube

$$\frac{P(\tau)}{P_{ideal}} = 1 - e^{-\alpha\tau}, \text{where}: \tau = \frac{t}{\left(L + L_{eff}\right)^{\gamma}}, \tag{4}$$

Here, the parameter α represents a characteristic value for the porous media, and it depends on aspects specific to the internal structure of the media such as the porosity, tortuosity and frictional coefficient. This value may be determined from a single characterization experiment to generate the shock transmission pressure trace behind the porous barrier. From equation (4), we may note that the

transmitted reflected pressure value, P(τ), given enough time will eventually reach the undisturbed reflected pressure value (P_{ideal}), which implies a complete pressure recovery. In the context of a Friedlander blast wave, where unlike a shock wave, the pressure decays immediately upon arrival of the wave front, the pressure value $P_{\max}(\tau)$ is expected to be lower than P_{ideal}, resulting in an attenuation in terms of the peak pressure as well.

Flow path. A review of both experimental and numerical studies of shock waves (M_s = 1.4–1.9) entering a region of sudden area change was provided by Abate and Shyy (2002). This work showed that the basic flow structures in the early times are very similar, regardless of whether the shock expands along one, two or three dimensions. This is expected to hold even for blast wave propagation. They also show that very little dissipation occurs within the flow structures, apart from the region near the expansion corner and the shock wave itself. High-strain rate regions due to vorticity that develops at later times, and dilation due to shock waves, were identified as the major causes for the dissipation.

Shock attenuation (M_s = 1.45) was studied through various configurations of double bend ducts with differing internal roughness (Igra et al., 2001). It was found that a bend of length L that was *four times* the shock propagation channel width (H) was the optimal value to maximize shock attenuation and minimize volume increase (or the occupied space). Roughness was also found to enhance attenuation. It was also shown that viscosity plays a role only in the later times and that an inviscid simulation is sufficient for the early times.

Instead of the 'attenuation by blockage' concept that was addressed thus far, a convoluted 'zigzag' path for the shock wave was numerically evaluated (Kumar and Pathak, 2020), with a view to developing a lightweight protective structure. The effective open passage for the flow, different from the projected open space, remains the same despite the convoluted path, giving a blockage ratio of *zero*. For purposes of comparison, staggered cylinders with a blockage ratio of 0.6 and a zigzag path with cylindrical obstacles resulting in a blockage ratio of 0.4 were used. The idea was to weaken the shock wave by repeated interactions with the convoluted wall, instead of a single reflection occurring off an obstacle block. For the first case, it was found that alternate reflection and diffraction occurring in the zigzag path contributed significantly to attenuation. In the second case, reflection off the cylindrical obstacle was the contributing factor, in addition to some attenuation arising from reflection, and diffraction off the cylinders in the downstream rows. In the last case, the presence of cylindrical obstacles added to the attenuation produced in the first case by means of the extra reflections off the cylinders. The attenuation measured in terms of incident and reflected pressure reductions was found to be increasing in this order (34%, 36% and 64%, respectively) showing that weight reduction may be achieved without compromising on the attenuation performance.

Figure 18 shows the test objects on which shock propagation studies have been carried out. It is to be noted that most or all of these studies were for shock waves. To understand the difference between the response to a blast wave and a shock wave, a few studies are available in the open literature and are briefly summarized in the next section.

Contrasting shock wave and blast wave interactions. Ritzel et al. (2018), as part of their studies on the drag loading of a free sphere, suggest that if shock wave loading were considered to be an unsteady flow problem, then blast wave loading ought to be considered a doubly unsteady flow problem. It is not always clear as to how shock tube-based experiments would correspond to a field explosion, as the duration and decay of the pulse are quite different. Ofengeim and Drikakis (1997) report

numerical studies on wave propagation behind infinitely tall cylinders for three types of waves having the same peak pressure value corresponding to M_s = 1.7:

- a shock wave ($t_d = \infty$, for mathematical consistency),
- a long duration blast wave (t_d = 15 ms) and
- a short duration blast wave (t_d = 3.2 ms).

The authors show that for the shorter duration blast waves the viscous–inviscid interactions are weaker, the shock front interactions are different at later times and the vortices do not move downstream. With regard to the peak initial pressure, the behaviour is expected to be similar, as Epstein and Kudryavtsev (2012) showed using CFD, but the applicability of shock tube experiments for impulse loading is still not clear. For instance, the contrasting results on the role of structural thickness in the attenuation brought about by a barrier – for a blast wave by Miura et al. (2013); and for a shock wave by Sha et al. (2014) – may be attributed to the non-consideration of curvature of the blast wave in the shock tube-based work of Sha et al. (2014). Nonetheless, it appears that shock wave based data are an excellent way to understand how the instantaneous pressure rise, which is also associated with a blast wave, may be mitigated.

Modelling realistic scenarios. A simple model of a railway station was studied by Hajek and Foglar (2015) with a view to understanding the role of obstacles in mitigating the pressures (Figure 19). However, no reduction in overpressure due to the barriers was observed both experimentally and numerically. The authors suggested that barriers are effective in reducing pressure only in a localized region in its vicinity and not in the far-field.

Gan et al. (2022) studied the influence of randomly placed obstacles on the development of pressure and impulse within an internal environment. They found that channelling is highly localized and results in increased loading near the explosive, the effect of which increases with obstacle density. Shielding was shown to be a cumulative effect which increases with distance from the explosive, and with increasing obstacle density.

General outlook on indirect loading: Obstacles

Shock tubes have been primarily employed to study the evolution of loading on different shapes of obstacles – individually, and as groups – as it is a convenient means to generate an instantaneous rising pressure load that is characteristic of any blast loading. For the loading of multiple obstacles, an important finding has been that the shape of the obstacle is of secondary importance. The dominant characteristic has been identified as the blockage ratio of the obstacles, that is, some measure of the restricted volume that the shock/blast has to propagate through. Additional concepts which may be incorporated in designing novel blast protection obstacles include a sudden volume expansion, a change of direction of the wave (zigzag path) and the use of perforations or rough-walls. The relevance of shock tube-based research for blast wave studies was also highlighted.

From the few studies modelling realistic scenarios, it appears that the shock attenuation observed at small scales do not fully translate to a full-field scenario. This is because the height of the obstacles, which were modelled as 2D in shock tubes, cannot be scaled up to infinity in the real world. Researchers therefore have begun to adapt to account for the inability to have tall (infinite) obstacles, by proposing a new combination of structures, termed here as hybrids, which form the topic of discussion for the next major section.

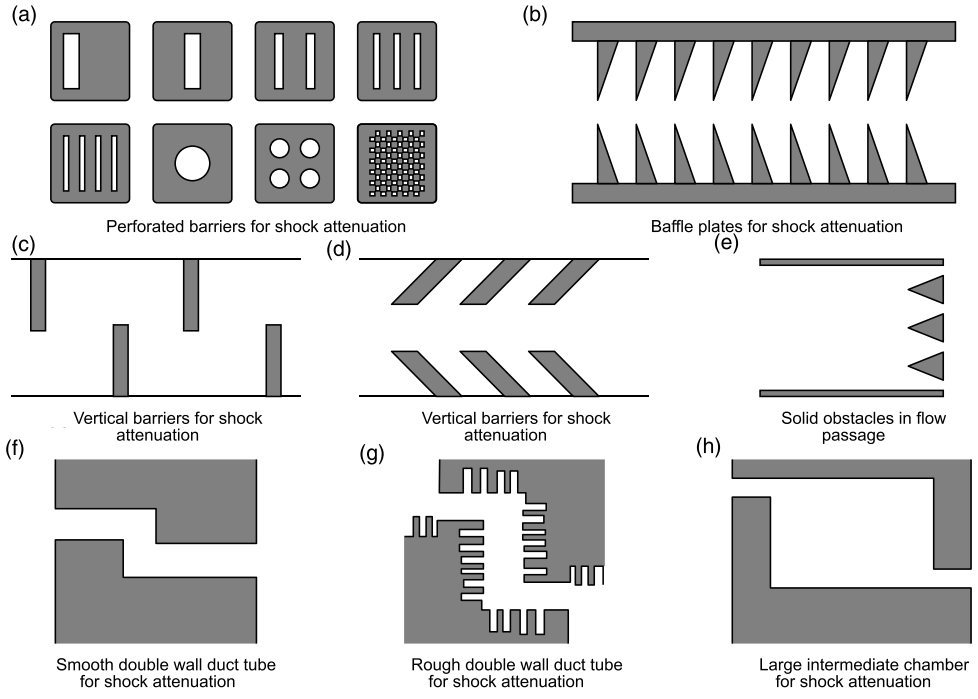

Figure 18. A selection of obstacles (a–h) that have been investigated as forms of shock attenuation as reported by Kumar and Pathak (2020).

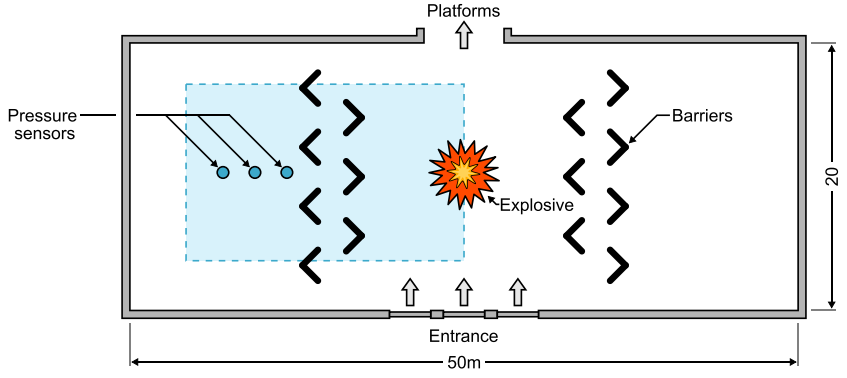

Figure 19. A schematic diagram of the layout used to simulate the effectiveness of barriers for attenuating the blast loading from an explosive detonated in a railway station building (Hajek and Foglar, 2015). The experimentally tested area is shaded blue.

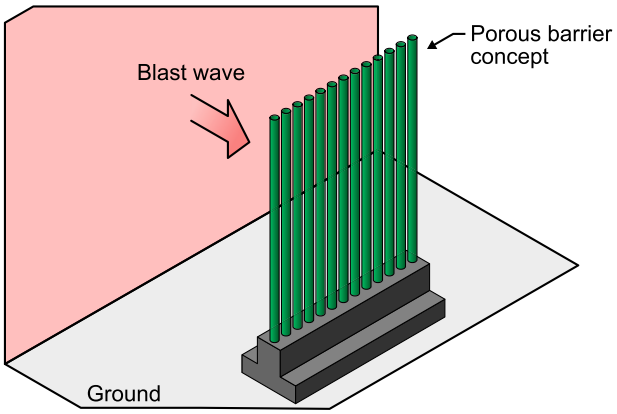

Figure 20. An illustration of the fence wall concept comprising obstacles (poles) spaced apart to create a hybrid (blast wall) which is a novel concept in passive blast wave mitigation.

Indirect loading: Hybrid types

Fence wall

The mechanism by which a barrier attenuates a blast wave is primarily due to diffraction, or the shadowing effect. For multiple obstacles having low porosity, it is a combination of the blockage induced by the obstacles, and the dissipation brought about by travelling through such constricted openings. Combining these two mechanisms, and arranging multiple obstacles like a barrier, one can have a realistic structure that can help mitigate an explosion in urban scenarios. This gave rise to the concept of what is now referred to as a 'fence wall' (Figure 20).

Gencel et al. (2015) studied the effectiveness of a 2 m long barrier comprising a series of 13 GFRP poles, each 2.5 m tall and having an outer diameter of 85 mm, as shown schematically in Figure 20. The aim of this study was to evaluate the effectiveness of protecting airport terminals using barriers whilst maintaining radio transparency. Experiments conducted using a 4 kg TNT equivalent explosive placed at a height of 1.5 m above the ground (to avoid reflections) showed promising results in terms of blast attenuation at stand-off distances ranging from 0.5 to 3.0 m.

Similarly, Zong et al. (2017) proposed the use of a fence wall concept using poles having various cross-sections for blast mitigation in a cityscape. Preliminary studies considered the shape of the obstacle, the spacing between obstacles, the effect of scaling up the dimensions, the obstacle layers and separation between the layers. Experimental validation of these numerical findings was then reported in a follow-up study (Hao et al., 2017). The authors suggest that although a square section generally performed better due to the stronger reflection that it generates, a circular section is to be preferred for reasons of better structural strength to weight ratio (Jin et al., 2019).

Xiao et al. (2018, 2020b) conducted experiments to study the role of increasing the number of square poles on the attenuation performance of a fence wall system. The aim was to understand the role of the relative opening fraction – similar to the concept of porosity – on blast mitigation. These experiments were used to validate a numerical model, which was then used to carry out subsequent optimization studies. It was found that a square shaped obstacle outperformed the other equivalent sized shapes (forward facing triangle, rear facing triangle and circle) that were considered. This mitigation, however, should be considered in conjunction with the fact that the loading on the barrier

was also increased, as previously noted by Zong et al. (2017). Xiao et al. (2018, 2020b) also observed an increasing mitigation as the number of poles were increased. Interestingly, multiple rows of poles were not shown to increase attenuation in their study. It is well known that spacing between poles in the first row is the controlling factor for downstream attenuation (Dosanjh, 1956). Since this was the same for both scenarios, it could perhaps explain why an enhanced attenuation was not observed.

Non-conventional techniques

Barriers such as bollards, benches, landscaping and plants are considerably less imposing than hardened structures such as blast walls. Accordingly, Gebbeken and Döge (2010) proposed the use of plants as barriers for attenuating a free-field blast wave. In a preliminary study carried out on different species of plants (Gebbeken et al., 2017), pressure reductions of up to 60% were shown to be possible, with most of the biomass remaining intact despite repeated impacts. Interestingly, the authors observed that the pressure profile changed from a typical Friedlander exponential decay to a shock wave-like flat-topped pressure profile. Criterion for the choice of plants, such as the use of narrow leaves (coniferous ones), and having a large biomass to account for inertial resistance, was formulated as part of this study. These experiments were conducted using 5 kg of TNT at approximately 5 m stand-off distance.

In subsequent experiments with a similar charge and sensor positioning but slightly different dimensions of the plants, a reduction of up to 45% in overpressure values were reported (Warnstedt and Gebbeken, 2020). Again, the authors did not observe a reduction in biomass (Yew and Thuja trees) after being impacted repeatedly by blast waves, although tilting was observed.[9] Bamboo and barberry exhibited a reduction of 30% in overpressure values behind the plants, but with significant reduction in biomass, thus rendering them less effective should there arise repeated explosion loads. The authors report, however, that this reduction in pressure is valid only up to a limited distance as the unimpeded blast wave travels over the plants and meets with the transmitted wave beyond a certain distance, leading to an almost complete recovery in pressures. Again, 5 kg TNT was used in these experiments, at a stand-off distance of 4 m. The sensors were placed approximately 1 m behind the plants and the overpressure reduction had almost halved at sensor locations that were just 0.5 m beyond. For example, for the Bamboo, it dropped from 28.8% to 9.9%; for the Yew, from 43.4% to 26% and for the Thuja, from 42.8% to 35.4% – an anomaly which could possibly be linked to the shock wave type profile behind these coniferous trees (Gebbeken et al., 2017), which do not decay as rapidly as the Friedlander-type waves. These plants were all approximately 2 m tall.

The role of trees in mitigating a blast wave were further explored recently by Gan et al. (2021) using a large shock tube blast wave simulator. Two Juniperus Spartan trees, 1.6 m high, were subjected to varying blast loads (25–50 kPa, $\sim$ 15 ms) and overpressure and impulse reductions of up to 20% were measured on a target wall behind the trees. Enclosing the trees in a wrap to make them less porous enhanced the attenuation performance, as the overall blockage ratio would go up. These trees were found to be resilient, and the trunk and most leaves were intact after 9 tests. The ability of the tree to continue to grow after exposure could not be tested as the trees were uprooted and embedded in concrete to perform the blast tests. For a similar range of explosive mass (5 kg) and stand-off distance (5 m), a steel mesh made up of rings of different sizes (with the potential to trap flying debris) was shown to help mitigate a blast wave (Gebbeken et al., 2018), and the inclusion of a water curtain indicated that further appreciable attenuation may be attained.

Using a similar test arrangement, another method was reported by Xiao et al. (2020a) using a wire mesh instead of an obstacle-based fence wall system. Although the reported attenuation of pressure

(up to 31%) was a little lower than what was measured for the barriers (Xiao et al., 2020b), it was found to render similar performance for a much lighter 'barrier' mass. Recently, a small-scale experiment using an explosive-driven shock tube was used to study the wave attenuation characteristics across a 'wire mesh' made of expanded metal (Schunck and Eckenfels 2021). The reference reflected pressure was around 20 bar, and the impulse was 3.2 bar-ms. The open area of each mesh was 24%, which gave rise to reduction of up to 75% (pressure) and up to 90% (impulse) when two layers of this perforated plate were used. Similar results were also reported at lower pressures (3 bar) for a free-field experiment, suggesting that this is a potential technique that could be used in a cityscape. Using two layers or even a single layer with water film over it helped increase the amount of wave reflection and this, according to the authors, helped improved the mitigation.

General outlook on indirect loading: Hybrid types

With a view to overcoming the limitations imposed by the other attenuation techniques, hybrid methods, which are a combination of barriers and obstacles, were briefly reviewed. Several successful hybrid methods are now available, viz., optimized fence walls, wire meshes/ring fences and even plants, all of which have been verified using field experiments and shown to provide mitigation of at least 20%, albeit for a limited region behind the obstacle. These methods have attempted to incorporate aspects of protective design which can fit into a cityscape without appearing to be disruptive or imposing, yet provide protection to the structures they aim to protect. In the next section, we review methods that are available to quantify the evolution of pressure loads due to a blast wave, for both direct and indirect loading scenarios.

Prediction tools

The determination of the blast load and structural response are carried out using either first principles methods like CFD, which solve the equations of motion according to the laws of physics. For certain simple scenarios, (semi-) empirical methods, derived either in-part or entirely using experimental data are relevant. Additionally, machine learning methods are increasingly being used in engineering applications, including blast load and response prediction.

Direct loading

For direct loading on structures, simple techniques may suffice for geometrically idealized settings. The more sophisticated approaches are only necessary for situations where the blast wave has been impeded by other obstacles or a barrier. As outlined in the section on direct loading, for certain scenarios, the free-field blast parameters may be directly used to estimate the load for certain structure and stand-off distance combinations. For such special cases, such as on isolated buildings at great distances from an explosion, the surface burst and/or air blast parameters may be calculated using a variety of semi-empirical techniques (Kinney, 1985; Kingery and Bulmash, 1984; Hyde, 1991). For a review of simplified techniques to predict blast loads, the reviewer is directed to Remennikov (2003).

For scenarios where a single value of clearing can be applied to the entire face, a simple correction was first proposed by Bleakney using shock tube experiments at Princeton in 1952. Additional details of this experiment may be found in Shin and Whittaker (2019). The correction is available in terms of the clearing time t_c (Norris et al., 1959), defined as the duration required for the

reflected pressure to decay to the stagnation pressure (Figure 3). This is estimated using the distance to an edge on the obstacle S and the shock velocity U as given in equation (5)

$$t_c = \frac{3S}{U} \tag{5}$$

A slightly improved variant of this formula was then included in the UFC 3-340-02 (US Department of Defence, 2008), with the clearing distance S taken to be $min\ (h, W/2)$, as illustrated in Figure 21. The improved formula is given in equation (6)

$$t_c = \frac{4S}{(1+R)C_r} \tag{6}$$

To obtain the structural response, SDOF-based techniques as recommended in TM5-1300 (US Army Corps of Engineers, 1990) can provide a good first estimate, and they can be readily adapted to implement cleared pressure values using the formulae in equations (5) and (6) and several similar ones as described in other detailed reviews on the topic (Bhatti et al., 2017; Ullah et al., 2017).

Indirect loading

The case of indirect loading is more complicated as it involves aspects such as shock reflection, diffraction and vorticity rather than the simple case of clearing. Accordingly, this often requires the use of a full CFD simulation. Nevertheless, given a porosity value for an obstacle configuration, some simple analysis carried out using 1D modelling can give insights into the final attenuation values.

Quasi-1D gas dynamics code for porous structures. Britan et al. (2006) report the use of a quasi-1D nozzle model to simulate the blockage introduced by a porous obstacle to the blast transmission. This involves numerically solving the relevant conservation equations for an unsteady inviscid flow in a quasi-1D geometry to obtain the pressure downstream of the nozzle. This value may then be correlated to the pressure behind a porous barrier. Good correspondence between the experimental data and the numerical results was observed, suggesting that this can be a quick method to accurately estimate average pressure history over a region.

Instead of the geometric area reduction that was simulated by Britan et al. (2006) for a blast wave travelling through a channel with packed cylinders, Suzuki et al. (2000) suggested the use of a drag force term in the 1D Euler equations. The drag force in the source term may be obtained either from an experiment, or using other empirical methods. This model was also found to perform well against experimental data.

As described earlier, Ram and Sadot (2013) proposed the use of a simple formula to obtain the pressure evolution over a wall placed at some distance from a rigid porous barrier impacted by a shock wave. A single shock loading experiment using a block of porous material would suffice to obtain the value of a bulk parameter (α) that encapsulates the porosity, tortuosity, friction loss etc. through the material. Inserting this value into equation (4) would then provide the pressure history on a wall beyond the porous barrier.

Since blast waves are usually a non-linear phenomenon, the advantage of these quasi-1D methods is that the actual conditions – shock speeds and overpressure values – are used, which will result in reproducing the flow conditions faithfully. It should be noted, however, that these are essentially single point data models, and so they cannot describe the spatial variation over the target.

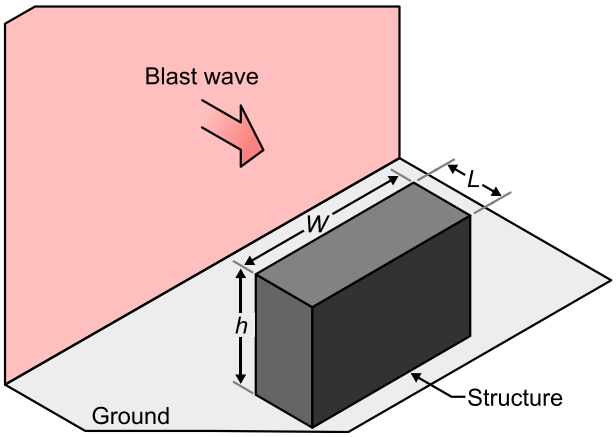

Figure 21. An illustration showing a blast wave impacting a finite-sized structure, for which the clearing distance is given by $S = min\ (h, W/2)$.

However, they can still provide reliable estimates of the pressure that a target surface would experience.

Empirical methods for barriers. As described earlier, the empirical formula for predicting the overpressure and impulse on a building face behind a barrier wall of a given height was first given by Chapman et al. (1995b) in terms of a modified scaled distance. The authors developed an empirical relationship between a modified form of reflected pressure (termed 'factored peak pressure', P_f) and a combined distance parameter that accounts for the total distance from charge to the target, the HoB, the wall height and the target height (termed 'protection factor', F_p). A similar relationship for 'factored peak impulse' was also used to arrive at a correlation for impulse, and all these are given in equation (7)

$$
\begin{aligned}
F_p &= (Z_{B,TNT} + Z_{T,TNT})\frac{H_B}{HoB \times H_t} \\
P_f &= P_r\frac{HoB + H_T}{(d_B + d_T) \times H_B} \\
i_f &= i_r\frac{(HoB + H_T)}{(d_B + d_T) \times H_B \times W^{1/3}} \\
&\textit{where}, \\
P_f &= 10^{2.881}F_p^{-2.363} \\
i_f &= 10^{2.155}F_p^{-2.399}
\end{aligned}
\tag{7}
$$

Zhou and Hao (2008) then generated a more comprehensive numerical simulation dataset that was used to derive an empirical formula for pressure, impulse, arrival time and decay time of the pressure load at each point on the wall. This methodology was then adapted for a fence wall barrier by Gencel et al. (2015). The work of Zhou and Hao (2008) was extended by Steven and Khaled

(2017) for frangible walls, by using a correction factor based on the effectiveness (in alleviating pressure and impulse) of 12 materials that were available in literature. This method was then compared with the VAPO software, and the results were found to be on the conservative side. The advantage, however, is in the extremely short time taken to arrive at the results, which will be useful to make a decision for or against a given concept in the preliminary stages of design. Other prediction methods for barriers, may be found in the review by Bhatti et al. (2017)

Heuristic/statistical – Prediction on the ground. Éveillard et al. (2013) presented a fast-running method for obtaining pressures on the ground behind a barrier having an inclined rear face, based on data from TM5-1300 (US Army Corps of Engineers, 1990). Estimates were made for the reflected shock pressures at points on the ground, based on the incident Mach number and the angle of incidence. For diffraction around the barrier edges, sample simulations were run to obtain attenuation coefficients based on deflection angle and incident Mach number. This was an improvement over the work of Miller (2004), who had used a single diffraction factor (0.35) for all cases. A simplified version of the LAMB model (Needham, 2010) was then used to combine the pressure contributions from multiple rays running from a source located on the ground and the symmetry plane of the barrier to obtain the pressure evolution at each point behind the barrier. The overpressure values predicted by the fast-running method were in the range of −30% to +100% of the numerical computation values, which was deemed reasonable for proof-of-concept studies.

Heuristic/statistical – Prediction on a target wall. A fast-running method also involving segregating the loading regions by using certain critical points (Zhou and Hao, 2008) along the height of the target wall was proposed by Sung and Chong (2020). Three points were identified along the height of the wall (Figure 22) to delineate the loading regions:

1. direct incident wave loading region;
2. incident wave and a single diffraction wave loading region and
3. at the lower portion of the target wall, where a reflected ground shock wave and both diffracted waves from two edges on the top of the barrier interact.

FEM simulations were used to optimally locate these points, and approximate calculations based off the KB relations were proposed. The reflected pressure predictions were found to be reliable unlike the impulse values, which they attributed to the inherent errors in the KB impulse predictions. The authors recommend the use of this technique for first estimates in designing a structure but suggest the use of advanced CFD software for a finer analysis.

Engineering models

The assessment of blast effects for buildings would require complex calculations involving high-level FEA or CFD, which are computationally very expensive and require expert users. However, there are certain engineering tools that are quick and are available for estimating the blast loading even for certain complex scenarios:

BlastX (Robert et al., 2001) and SHOCK (Wager, 2005) are extended semi-empirical engineering codes which can provide blast loading estimates for either external or internal scenarios such as the calculation of explosion parameters inside a chamber bound by 1–4 reflecting surfaces.

The Vulnerability Assessment and Protection Option (VAPO) program as an integrated environment can provide a rapid characterization, analysis and vulnerability assessment for complex

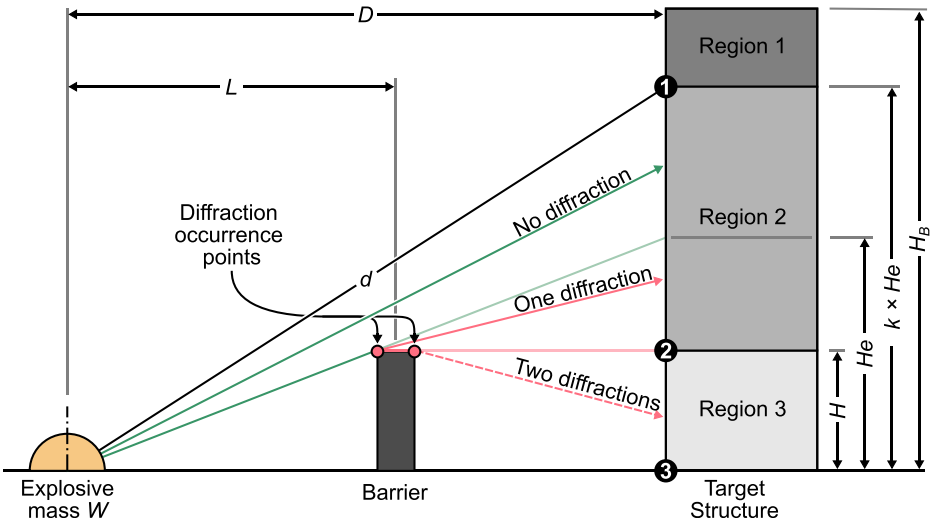

Figure 22. A schematic detailing the critical points (1–3) on a target structure loaded by an explosive charge detonated behind a barrier wall. Figure taken from Sung and Chong (2020).

urban environments such as landscape sites, buildings and vehicles while using semi-empirical formulas to generate the blast loading (Nichols and Doyle, 2014).

Another program which utilizes the curve fits data extracted from TM5-1300 (US Army Corps of Engineers, 1990) is called VecTor-Blast (Miller, 2004). It can produce the blast loading parameters such as pressure, impulse and Mach number acting on cuboid structure using ray path method considering reflection, diffraction and Mach phenomenon.

Deep learning methods

Remennikov and Rose (2007) used experimental data and an artificial neural network (ANN) to predict the pressure and impulse contours in the region behind a barrier where protection is intended. The input parameters were the scaled value of stand-off distance, charge elevation, distance behind the wall, height of the barrier and height of the point of interest. Having trained a model and validated it, they also showcase how such a contour plot may be used by the designer to adjust the location and height of the barrier to enhance protection at the intended location. An ANN (using a radial Gaussian architecture with an incremental learning paradigm) was trained using an extended dataset, generated using DYSMAS software, to predict roof loads on a simple building (Bewick et al., 2011). The pressure and arrival time were predicted quite well, but the non-linearity in the impulse and decay time values made it more challenging. Nevertheless, the ANN was shown to be able to predict the roof loads on the building within a fraction of a second, making it a promising technique for future fast-running codes. Recently, the use of ANNs for confined loading (Dennis et al., 2020) and for near-field loading (Pannell et al., 2021, 2022a, 2022b) were also successfully demonstrated.

In order to obtain the post-explosion blast environment in an urban space, one can perhaps consider dividing the physical space into a digital space, where a binary system may be used to specify the presence or absence of a building/structure as part of the input conditions. This is similar to what was proposed in Zhang et al. (2021) for a different problem. It is to be noted that these fast-

running methods and deep learning based techniques are for blast evolution behind a barrier. Such techniques are still not available for the more complex case of flow around an obstacle, as the 3D effect would then start dominating.

Computational fluid dynamics (CFD)

Smith and Rose (2006) suggested that well-resolved, three-dimensional CFD analyses of blast wave propagation in complex urban environments will be commonplace among the structural engineering community 'within a few years'. Since then, several CFD solvers have been developed, each with their specific strengths and limitations. A non-exhaustive list may be found in Table 3.

Each of these is characterized by various methods of solving the governing equations (conservation equations and equations of state) of fluid flow for a given set of initial and boundary conditions. They may differ in terms of the methodology of solving the temporal equations, which can use either an explicit or an implicit type solver; the solution may be computed either on a structured grid or on an unstructured one; the frame of reference for the motion could be one of Lagrangian (Lag), Eulerian (Eul) or an Arbitrary Lagrangian Eulerian (ALE). Additionally, the method of initializing the blast load; the scope of including after-burn models (Af-B); the ability to map the solution from an initial mesh to a different one (Remap); the provision of automatic mesh refinement (AMR) which can reduce the computational time and fluid–structure interaction capabilities (FSI) which can couple the structural and fluid dynamic solvers can also differ. A summary of capabilities of these solvers may be found in Table 4.

Initialization. In any CFD simulation, the procedure to initiate the solution is an important aspect of the process and may be done by one of the following methods: using the mass of the explosive and modelling the detonation process in the solid explosive; using a compressed balloon of (hot) gas to initiate the solution; remapping data from a previous numerical solution; using ConWep data or other semi-empirical models and using a pre-defined pressure time curve. The interested reader may refer to the review of Larcher and Casadei (2010).

Material models. The equation of state (EOS) (Éveillard et al., 2013) and material model (Langlet et al., 2015) should be carefully chosen to simulate the explosive and the surrounding medium, especially in the events consisting of a large explosive mass and for cases where near-field detonation is the focus (Hao et al., 2016). The explosive charge shape, orientation and detonation initiation point should be taken into account, especially when modelling near-field detonation as charge shape can affect the overpressure distributions.

Boundary conditions. Careful attention should also be paid to the choice of boundary conditions. For example, to recreate a symmetric planar experiment involving an explosion, a semi-infinite barrier and the target wall (Chapman et al., 1995b), numerical validation using AUTODYN (Chapman et al., 1995a) was successfully carried out using an axisymmetric model. This, according to the authors, is a better technique when compared to using a planar symmetry for the numerical model as it avoids overestimation. Symmetry planes may also be exploited in order to perform experimental studies in reduced dimensions, for example, quarter-symmetry (Anthistle et al., 2016).

Other considerations. The choice between Eulerian or Lagrangian and coupled or uncoupled approaches is critical in cases where the structure can deform and offer resistance when internal pressure rises suddenly (Børvik et al., 2009).

The model can be explicitly or implicitly solved in time, depending on the type of the software. For more details on the solution process and the advantages and disadvantages of each type, the reader is referred to the review paper by Hao et al. (2016). Although CFD computes the solution from first principles, an experimental validation is always necessary as the solution process includes detonation and turbulence models that are not always from first principles. The size of the mesh (Remennikov and Rose, 2005; Benselama et al., 2010) and the number of mesh elements per physical object (Remennikov and Rose, 2007) all contribute to the validity and fidelity of a solution. Therefore, carrying out a mesh sensitivity analysis and validating numerical results against experiments is an essential aspect of any simulation.

Outlook/summary

In the mid-19th century, engineers tasked with designing structures for resilience against blast effects would have been considering situations of relative simplicity: large-scale (e.g. nuclear) blasts, detonated at large distances from the target structure. Simple formulations, available in textbooks and design codes, were thus sufficient to specify the loading that the structure would be subjected to. Since then, with a marked increase in both terrorist activity and urbanization, the challenge has shifted to smaller, targeted explosions in crowded urban environments. To this end,

Table 3. A list of common software in use for blast interaction studies.

Computer code	Developer
ABAQUS	ABAQUS Inc. (Mougeotte et al., 2010)
APOLLO blastsimulator	Fraunhofer, EMI (Fra, 2018)
AUTODYN	Century Dynamics, ANSYS (Fairlie, 1998)
blastFoam	Synthetik Applied Technologies (Heylmun et al., 2019)
CTH	Sandia National Laboratories (McGlaun et al., 1990)
LS-Dyna	Livermore Software Technology, ANSYS (Hallquist, 2006)
ProSAir	Cranfield University (Cra, 2009)
SHAMRC	Applied Research Associates, Inc. (Crepeau et al., 2001)

Table 4. A compilation of capabilities of common CFD software.

	Solver type		Discretization						
Software	Implicit	Explicit	Lag	Eul	ALE	Remapping	AMR	FSI	Af-B
Abaqus/CEL		✓	✓	✓	✓		✓	✓	
Apollo blastsimulator		✓		✓		1D:3D	✓	✓	✓
AutoDyn		✓	✓	✓	✓	1D: 2D:3D		✓	✓
blastFoam		✓	✓	✓		1D: 2D: 3D	✓	✓	✓
CTH		✓	✓	✓		1D:2D:3D	✓	✓	
LS-Dyna	✓	✓	✓	✓	✓	1D: 2D:3D	✓	✓	
ProSAir		✓		✓		1D: 2D: 3D			
SHAMRC		✓		✓		2D:3D	✓		✓

proximal blast loading on shapes such as parallelepipeds, cylindrical columns and spheres have been studied using both shock tubes and field experiments. The role played by clearing in reducing the overpressure load was elucidated, and the availability of an improved formula has been identified.

Solid barriers have been studied, and some correlations to assist the designer are available in various forms. The role of a canopy over the barrier has also been investigated and found to be effective in mitigating blast pressure. Shock tubes have been used to study effectively infinite length obstacles, and some concepts for pressure mitigation may be incorporated into the design of (high explosive) blast protection strategies in the urban environment. Although the overpressure is almost always lowered in the wake of a rigid blast wall-type obstacle, increases in impulse have been observed in certain regions, attributed to diffracted wave interaction and coalescence. Thus, a holistic approach should be taken when considering the role of protective barriers and obstacles. Furthermore, the risk of fragmentation of frangible barriers cannot be neglected.

Wave disruption by using intermediate-scale obstacles to reduce the loading on target is another possible attenuation technique for urban scenarios. Strategies such as poles, wire meshes, plants and water jets have been implemented in past studies, and it is generally found that these strategies are highly effective at mitigating near-field blast loading (higher Mach numbers). A significant finding in these studies is that the blockage ratio is the single most important factor in dictating the level of mitigation, while other factors such as shape, number of obstacles and rows, and arrangement, play a secondary role. Key mechanisms governing blast attenuation were identified as diffraction, reflection (diverting away from the target structure), expansion/volume increase, vortex creation/growth, porosity and surface roughness.

Finally, a number of quick-running engineering tools were reviewed. These enable the designer to rapidly analyse a comprehensive parameter space with little computational expense. The accuracy of such methods varies; however, their suitability for scoping and probabilistic studies is clear. Sophisticated machine learning methods, trained using datasets from comprehensive physics-based modelling studies and/or experimental work, provide an interesting outlook for the development of predictive approaches in this area since they potentially balance the accuracy of FEM/CFD with the low computational expense of quick-running engineering tools.

Declaration of conflicting interests

The author(s) declared no potential conflicts of interest with respect to the research, authorship, and/or publication of this article.

Funding

The author(s) disclosed receipt of the following financial support for the research, authorship, and/or publication of this article: This work was supported by the UK Engineering and Physical Sciences Research Council (EPSRC) grant EP/S037241/1.

ORCID iDs

Obed Samuelraj Isaac https://orcid.org/0000-0003-3621-5903
Omar Ghareeb Alshammari https://orcid.org/0000-0003-3419-8054
Samuel David Clarke https://orcid.org/0000-0003-0305-0903
Samuel Edward Rigby https://orcid.org/0000-0001-6844-3797

Notes

1. N.B.: the blast wave duration increases with distance, however, the impulse of the blast wave, which is the temporal integral of pressure with respect to time, also reduces as the reduction in pressure with distance is much more substantial than the increase in duration.
2. As the scaled stand-off distance increases, it tends to be an acoustic interaction.
3. Usually ignored, as *CD* is taken to be 1 for the front face.
4. Except under a narrow set of conditions (Monti, 1970).
5. Depending on the curvature of the incident wave.
6. Incidentally, this is how the structure for an incident blast pressure sensor is designed (Sachs and Cole, 1976).
7. $S < Z/250$.
8. Although these obstacles (Figure 16) can be taken to be the front face of the barrier, the results should be equally valid for a canopy as well.
9. The plants were not grown in the soil but were transplanted to the test site, back-filled with sandy soil which was then watered and compacted to minimize tilting.

References

Abate G and Shyy W (2002) Dynamic structure of confined shocks undergoing sudden expansion. *Progress in Aerospace Sciences* 38(1): 23–42.

Anthistle T, Fletcher D and Tyas A (2016) Characterisation of blast loading in complex, confined geometries using quarter symmetry experimental methods. *Shock Waves* 26: 749–757.

Aune V, Valsamos G, Casadei F, et al. (2017) On the dynamic response of blast-loaded steel plates with and without pre-formed holes. *International Journal of Impact Engineering* 108: 27–46.

Baker W E (1973) *Explosions in Air*. Austin, TX: University of Texas Press.

Ballantyne GJ, Whittaker AS, Dargush GF, et al. (2010) Air-blast effects on structural shapes of finite width. *Journal of Structural Engineering* 136(2): 152–159.

Barakat MA and Hetherington JG (1998) New architectural forms to reduce the effects of blast waves and fragments on structures*Under Shock and Impact V. WIT Transactions on The Built Environment*: 53–62.

Barakat MA and Hetherington JG (1999) Architectural approach to reducing blast effects on structures. *Proceedings of the Institution of Civil Engineers - Structures and Buildings*.

Bazhenova TV, Gvozdeva LG and Nettleton MA (1984) Unsteady interactions of shock waves. *Progress in Aerospace Sciences* 21: 249–331.

Benselama AM, William-Louis MJP and Monnoyer F (2010) Prediction of blast wave effects on a developed site. *International Journal of Impact Engineering* 37(4): 385–396.

Berger S, Ben-Dor G and Sadot O (2015) Experimental and numerical investigation of shock wave attenuation by dynamic barriers. *Journal of Fluids Engineering* 138(3).

Beshara FBA (1994a) Modelling of blast loading on aboveground structures–I. General phenomenology and external blast. *Computers & Structures* 51(5): 585–596.

Beshara FBA (1994b) Modelling of blast loading on aboveground structures–II. Internal blast and ground shock. *Computers & Structures* 51(5): 597–606.

Bewick B, Flood I and Chen Z (2011) A neural-network model-based engineering tool for blast wall protection of structures. *International Journal of Protective Structures* 2(2): 159–176.

Beyer ME (1986) 'Blast Loads behind Vertical Walls', Prepared for Twenty-Second DoD Explosives Safety Seminar Anaheim.

Bhatti AQ, Badshah E, Naseer A, et al. (2017) Review of blast loading models, masonry response, and mitigation. *Shock and Vibration* 2017: 6708341.

Biggs J M (1964) *Introduction to Structural Dynamics*. New York, NY: McGraw-Hill.

Børvik T, Hanssen AG, Langseth M, et al. (2009) Response of structures to planar blast loads - a finite element engineering approach. *Computers & Structures* 87(9): 507–520.

Britan A, Igra O, Ben-Dor G, et al. (2006) Shock wave attenuation by grids and orifice plates. *Shock Waves* 16(1): 1–15.

Bryson AE and Gross RWF (1961) Diffraction of strong shocks by cones, cylinders, and spheres. *Journal of Fluid Mechanics* 10(1): 1–16.

Chapman TC, Rose TA and Smith PD (1995a) Blast wave simulation using AUTODYN2D: A parametric study. *International Journal of Impact Engineering* 16(5): 777–787.

Chapman TC, Rose TA and Smith PD (1995b) Reflected blast wave resultants behind cantilever walls: A new prediction technique. *International Journal of Impact Engineering* 16(3): 397–403.

Chaudhuri A, Hadjadj A, Sadot O, et al. (2013) Numerical study of shock-wave mitigation through matrices of solid obstacles. *Shock Waves* 23(1): 91–101.

Christiansen AP and Bogosian DD (2012) Limitations and consequences of fragment protection for near-field airblast measurements. *83rd Shock & Vibration Symposium*.

Codina R H, Ambrosini D and de Borbón F (2013) Numerical study of confined explosions in urban environments. *International Journal of Protective Structures* 4(4): 591–617.

Coughlin A, Musselman E, Schokker A, et al. (2010) Behavior of portable fiber reinforced concrete vehicle barriers subject to blasts from contact charges. *International Journal of Impact Engineering* 37(5): 521–529.

Cra (2009) ProSAir Propagation of Shocks in Air (A Computational Fluids Dynamics Code Developed by the Department of Engineering Systems and Management).

Craig J E (1977) *Weak Shocks in Open-Ended Ducts with Complex Geometry, PhD Thesis*. Pasadena, CA: California Institute of Technology.

Crepeau J, Needham C and Hikida S (2001) *SHAMRC Second-Order Hydrodynamic Automatic Mesh Refinement Code*. Albuquerque, NM: Applied Research Associates.

Dennis AA, Pannell JJ, Smyl DJ, et al. (2020) Prediction of blast loading in an internal environment using artificial neural networks. *International Journal of Protective Structures* 12(3): 287–314.

Dey S, Murugan T and Chatterjee D (2020) Blast wave interaction with generic objects and the measurement of blast wave reattachment distances. *Journal of The Institution of Engineers (India): Series C* 101(5): 747–760.

Dosanjh DS (1956) *Interaction of Grids with Traveling Shock Waves, Techreport 3680*. Washington, DC: Johns Hopkins University.

Epstein DB and Kudryavtsev AN (2012) Shock and blast wave propagation through a porous barrier. In: K. Kontis (ed) *28th International Symposium on Shock Waves*. Berlin, Heidelberg: Springer Berlin Heidelberg, 537–542.

Éveillard S, Lardjane N, Vinçont J-Y, et al. (2013) Towards a fast-running method for blast-wave mitigation by a prismatic blast wall. *Comptes Rendus Mécanique* 341(8): 625–635.

Fairlie G (1998) *The Numerical Simulation of High Explosives Using AUTODYN-2D & 3D*. Institute of Explosive Engineers 4th Biannual Symposium, 743–751. Available at: http://truegrid.com/paper052f.pdf.

FEMA (2007) *Site and Urban Design for Security–Guidance against Potential Terrorist Attacks*. Washington, DC: FEMA. Technical report.

Fouchier C, Laboureur D, Youinou L, et al. (2017) Experimental investigation of blast wave propagation in an urban environment. *Journal of Loss Prevention in the Process Industries* 49: 248–265.

Fra (2018) Apollo Blastsimulator Manuel.

Gan ECJ, Remennikov A and Ritzel D (2021) Investigation of trees as natural protective barriers using simulated blast environment. *International Journal of Impact Engineering* 158: 104004.

Gan K, Brewer TR, Pope DJ, et al. (2022), Probabilistic analysis of blast-obstacle interaction in a crowded internal environment.

Gauch H L, Bisio V, Rossin S, et al. (2019) Predictions of the transient loading on box-like objects by arbitrary pressure waves in air. *Proceedings of the Royal Society A: Mathematical, Physical and Engineering Sciences* 475(2229): 20190360.

Gebbeken N and Döge T (2010) Explosion protection—Architectural design, urban planning and landscape planning. *International Journal of Protective Structures* 1(1): 1–21.

Gebbeken N, Rüdiger L and Warnstedt P (2018) Urbane sicherheit bei explosionen - schutz durch ringgeflecht mit wasser. *Bautechnik* 95(7): 463–476.

Gebbeken N, Warnstedt P and Rüdiger L (2017) Blast protection in urban areas using protective plants. *International Journal of Protective Structures* 9(2): 226–247.

Gencel O, Asprone D, Prota A, et al. (2015) Behavior of full-scale porous gfrp barrier under blast loads. *International Journal of Polymer Science*: 349310.

Glasstone S and Dolan PJ (1977) *The Effects of Nuclear Weapons*. Washington, DC: U.S. Department of Defense.

Hahn A, Mensinger M and Rutner M (2020) Peak overpressure and impulse due to diffraction over a cylinder and/or multi-reflection of a shock wave in structural design- Part I. *International Journal of Protective Structures*: 2041419620918883.

Hajek R and Foglar M (2015) Numerical and experimental analysis of the effect of rigid barriers on blast wave propagation. *Journal of Structural Engineering* 141: 04015061.

Hajek R, Foglar M and Fladr J (2016) Influence of barrier material and barrier shape on blast wave mitigation. *Construction and Building Materials* 120: 54–64.

Hallquist JO (2006) *LS-DYNA Theory Manual*. Livermor, CA: Livermore Software Technology Corporation, CA.

Hao H, Hao Y, Li J, et al. (2016) Review of the current practices in blast-resistant analysis and design of concrete structures. *Advances in Structural Engineering*.

Hao Y, Hao H, Shi Y, et al. (2017) Field testing of fence type blast wall for blast load mitigation. *International Journal of Structural Stability and Dynamics* 17: 1–22.

Heylmun J, Vonk P and Brewer T (2019) blastFoam Theory and User Guide.

Honghui S and Yamamura K (2004) The interaction between shock waves and solid spheres arrays in a shock tube. *Acta Mechanica Sinica* 20(3): 219–227.

Hudson C (1955) *Sound Pulse Approximations to Blast Loading (With Comments on Transient Drag), Techreport SC-TM-191-55-5*. Albuquerque, NM: Sandia Corporation.

Hyde D (1991) *Conventional Weapons Program (ConWep)*. Vicksburg, MS: US Army Waterways Experimental Station.

Igra O, Falcovitz J, Houas L, et al. (2013) Review of methods to attenuate shock/blast waves. *Progress in Aerospace Sciences* 58: 1–35.

Igra O, Wu X, Falcovitz J, et al. (2001) Experimental and theoretical study of shock wave propagation through double-bend ducts. *Journal of Fluid Mechanics* 437(210892261): 255–282.

Ivanov A, Fassardi N, Scafidi C, et al. (2019) Shock wave attenuation using rigid obstacles with large- and small-scale geometrical features. *Multiscale and Multidisciplinary Modeling, Experiments and Design* 2: 269–279.

Jin M, Hao Y and Hao H (2019) Numerical study of fence type blast walls for blast load mitigation. *International Journal of Impact Engineering* 131: 238–255.

Johansson M, Larsen OP, Laine L, et al. (2007), Explosion at an intersection in an urban environment-experiments and analyses.

Kingery CN and Bulmash G (1984) *Airblast Parameters from TNT Spherical Air Burst and Hemispherical Surface Burst*. Aberdeen Proving Ground, MD: TR 02555Ballistics Research Laboratory.

Kinney GF (1985) Explosive shocks in air. In: FK Gilbert and JG kenneth (eds). 2nd edition. Berlin, Germany: Springer.

Kumar RA and Pathak V (2020) Shock wave mitigation using Zig-Zag structures and cylindrical obstructions. *Defence Technology*.

Langlet A, Souli M, Aquelet N, et al. (2015) Air blast reflecting on a rigid cylinder: simulation and reduced scale experiments. *Shock Waves* 25(1): 47–61.

Larcher M and Casadei F (2010) Explosions in complex geometries — a comparison of several approaches. *International Journal of Protective Structures* 1(2): 169–195.

Liepmann H and Roshko A (2013) *Elements of Gas Dynamics, Dover Books on Aeronautical Engineering*. Mineola, NY: Dover Publications. https://books.google.co.in/books?id=IWrCAgAAQBAJ.

Makki EA (2017) *Experimental Studies on Mitigating the Risk of Air Blast Loading, Open Access Dissertations. Paper 601*. Kingston, RI: University of Rhode Island.

Mays GC, Hetherington JG and Rose TA (1999) Response to blast loading of concrete wall panels with openings. *Journal of Structural Engineering* 125(12): 1448–1450.

McGlaun J, Thompson S and Elrick M (1990) CTH: a three-dimensional shock wave physics code. *International Journal of Impact Engineering* 10(1–4): 351–360.

Miller P (2004) *Towards the Modelling of Blast Loads on Structures, Master's Thesis*. Toronto, ON: University of Toronto.

Miura H, Matsuo A and Tabuchi G (2013) Numerical investigation for pressure mitigation effects of dike on blast wave. *Journal of Loss Prevention in the Process Industries* 26(2): 329–337.

Monti R (1970) Normal shock wave reflection on deformable solid walls. *Meccanica* 5(4): 285–296.

Mougeotte C, Carlucci P, Recchia S, et al. (2010) *Novel Approach to Conducting Blast Load Analyses Using Abaqus/Explicit-CEL, Technical Report*. Arsenal, NJ: Army Armament Research Development And Engineering Center, Picatinny.

Mulligan P (2018) Shock wave interaction with a cylindrical structure. *AIP Conference Proceedings* 1979(1): 160019.

Needham C E (2010) *Blast Waves*. Berlin, Heidelberg: Springer.

Nichols J and Doyle G (2014) Current engineering models and capabilities in the vulnerability assessment and protection option (VAPO) software. *Structures Congress*.

Niollet JE, Yuen SCK and Nurick GN (2015) A study to assess the use of cylindrical bars as blast barriers. *International Journal of Protective Structures* 6(2): 263–286.

Norris CH, Hansen R J, Myle J Holley J, et al. (1959) *Structural Design for Dynamic Loads*. New York, NY: McGraw-Hill Book Company, Inc.

Ofengeim D K and Drikakis D (1997) Simulation of blast wave propagation over a cylinder. *Shock Waves* 7(5): 305–317.

Pannell J, Panoutsos G, Cooke S B, et al. (2021) Predicting specific impulse distributions for spherical explosives in the extreme near-field using a gaussian function. *International Journal of Protective Structures* 12(4): 437–459.

Pannell J, Rigby S and Panoutsos G (2022a) Physics-informed regularisation procedure in neural networks: an application in blast protection engineering. *International Journal of Protective Structures*. (accepted).

Pannell J, Rigby S and Panoutsos G (2022b) Application of transfer learning for the prediction of blast impulse. *International Journal of Protective Structures*. (accepted).

Payne T, Williams A, Worfolk T, et al. (2016) Numerical investigation into the influence of cubicle positioning in large-scale explosive arena trials. *International Journal of Protective Structures* 7(4): 547–560.

Prasanna Kumar SS, Patnaik BSV and Ramamurthi K (2018) Prediction of air blast mitigation in an array of rigid obstacles using smoothed particle hydrodynamics. *Physics of Fluids* 30(4): 046105.

Qasrawi Y and Heffernan PJ (2016) Improved procedure for calculating the cleared pressure acting on a finite target due to a mid-field blast. *International Journal of Protective Structures* 7(3): 305–324.

Qasrawi Y, Heffernan PJ and Fam A (2015) Numerical determination of equivalent reflected blast parameters acting on circular cross sections. *International Journal of Protective Structures* 6(1): 1–22.

Qi S, Zhi X, Fan F, et al. (2020) Propagation behaviour of a hemispherical blast wave on a dome roof. *Engineering Structures* 212: 110524.

Ram O and Sadot O (2013) A simple constitutive model for predicting the pressure histories developed behind rigid porous media impinged by shock waves. *Journal of Fluid Mechanics* 718: 507–523.

Remennikov A (2003) A review of methods for predicting bomb blast effects on buildings. *Journal of Battlefield Technology* 6(3).

Remennikov AM and Rose TA (2005) Modelling blast loads on buildings in complex city geometries. *Computers & Structures* 83(27): 2197–2205.

Remennikov AM and Rose TA (2007) Predicting the effectiveness of blast wall barriers using neural networks. *International Journal of Impact Engineering* 34(12): 1907–1923.

Rickman DD and Murrell DW (2006) Development of an improved methodology for predicting airblast pressure relief on a directly loaded wall. *Journal of Pressure Vessel Technology* 129(1): 195–204.

Rigby SE, Chaudhary N, Bogosian D, et al. (2017a) Large-scale validation of Hudson clearing predictions. In: Proceedings of The 17th International Symposium for the Interaction of Munitions with Structures (ISIEMS17), Bad Neuenahr, Germany.

Rigby SE, Lodge TJ, Alotaibi S, et al. (2020) Preliminary yield estimation of the 2020 beirut explosion using video footage from social media. *Shock Waves* 30(6): 671–675.

Rigby SE, Tyas A and Bennett T (2012) Single-degree-of-freedom response of finite targets subjected to blast loading – the influence of clearing. *Engineering Structures* 45: 396–404.

Rigby S E, Tyas A and Bennett T (2014a) Elastic-plastic response of plates subjected to cleared blast loads. *International Journal of Impact Engineering* 66: 37–47.

Rigby SE, Tyas A, Bennett T, et al. (2014b) A numerical investigation of blast loading and clearing on small targets. *International Journal of Protective Structures* 5(3): 253–274.

Rigby SE, Tyas A, Bennett T, et al. (2013) Clearing effects on plates subjected to blast loads. *Proceedings of the Institution of Civil Engineers - Engineering and Computational Mechanics* 166(3): 140–148.

Rigby SE, Tyas A, Clarke SD, et al. (2017b) Approach to developing design charts for quantifying the influence of blast wave clearing on target deformation. *Journal of Structural Engineering* 143(1): 04016150.

Ritzel DV, Van Albert S, Sajja V, et al. (2018) Acceleration from short-duration blast. *Shock Waves* 28(1): 101–114.

Robert BJ, Ranta DE and Joachim CE (2001) BlastX Code*, Version 4.2, User's Manual*. Vicksburg, MS: ERDC edn, US Army Engineer Research and Development Center. GSL TR-01-2.

Rose TA, Smith PD and May JH (2006) The interaction of oblique blast waves with buildings. *Shock Waves* 16(1): 35–44.

Rose TA, Smith PD and Mays GC (1995) The effectiveness of walls designed for the protection of structures against airblast from high explosives. *Proceedings of the Institution of Civil Engineers - Structures and Buildings* 110(1): 78–85.

Rose TA, Smith PD and Mays GC (1997) Design charts relating to protection of structures against airblast from high explosives. *Proceedings of the Institution of Civil Engineers - Structures and Buildings* 122(2): 186–192.

Rose TA, Smith PD and Mays GC (1998) Protection of structures against airburst using barriers of limited robustness. *Proceedings of the Institution of Civil Engineers - Structures and Buildings* 128(2): 167–176.

Sachs DC and Cole E (1976) *Air Blast Measurement Technology, Contractor Report DNA 4115F*. Colorado Springs , Colorado, USA: Defence Nuclear Agency, Kaman Sciences Corp.

Santos F, Larcher M, Valsamos G, et al. (2018) Access control points: reducing a possible blast impact by meandering. *Advances in Civil Engineering* 2018: 3506892.

Sasoh A, Matsuoka K, Nakashio K, et al. (1998) Attenuation of weak shock waves along pseudo-perforated walls. *Shock Waves* 8(3): 149–159.

Schunck T and Eckenfels D (2021) Experimental study of explosion mitigation by deployed metal combined with water curtain. *Applied Sciences* 11(14).

Seeraj S and Skews BW (2009) Dual-element directional shock wave attenuators. *Experimental Thermal and Fluid Science* 33: 503–516.

Sha S, Chen Z and Jiang X (2014) Influences of obstacle geometries on shock wave attenuation. *Shock Waves* 24: 573–582.

Shi Y, Hao H and Li Z-X (2007) Numerical simulation of blast wave interaction with structure columns. *Shock Waves* 17(1): 113–133.

Shin J and Whittaker AS (2019) Blast-wave clearing for detonations of high explosives. *Journal of Structural Engineering* 145(7): 04019049.

Skews BW, Draxl MA, Felthun L, et al. (1998) Shock wave trapping. *Shock Waves* 8(1): 23–28.

Smith P (2010) Blast walls for structural protection against high explosive threats: A review. *International Journal of Protective Structures* 1(1): 67–84.

Smith PD and Rose TA (2006) Blast wave propagation in city streets—an overview. *Progress in Structural Engineering and Materials* 8(1): 16–28.

Smith PD, Rose TA, Krahe SL, et al. (2003) Façade failure effects on blast propagation along city streets. *Proceedings of the Institution of Civil Engineers - Structures and Buildings* 156(4): 359–365.

Smith P, Rose T and Ng S (2004) 'The Influence of Areal Density on the Shielding and Channelling of Blast by Buildings'. 18th International Symposium on Military Aspects of Blast and Shock.

Steven S and Khaled E-R (2017) Quantifying blast effects on constructed facilities behind blast walls. *Journal of Performance of Constructed Facilities* 31(4): 04017027.

Sugiyama Y, Wakabayashi K, Matsumura T, et al. (2015) Effect of a small dike on blast wave propagation. *Science and Technology of Energetic Materials* 76(4).

Sung S-H and Chong J-W (2020) A fast-running method for blast load prediction shielding by a protective barrier. *Defence Technology* 16(2): 308–315.

Suzuki K, Himeki H, Watanuki T, et al. (2000) Experimental studies on characteristics of shock wave propagation through cylinder array. *The Institute of Space and Astronautical Science* 676.

Trélat S, Sochet I, Autrusson B, et al. (2007) Strong explosion near a parallelepipedic structure. *Shock Waves* 16(4): 349–357.

Trélat S, Sturtzer M-O and Eckenfels D (2020) Multi-scale experimental study of blast propagation around a hemi-cylindrical barrier. *WIT Transactions on The Built Environment* 198: 53–64.

Tyas A, Warren JA, Bennett T, et al. (2011) Prediction of clearing effects in far-field blast loading of finite targets. *Shock Waves* 21(2): 111–119.

Ullah A, Ahmad F, Jang H-W, et al. (2017) Review of analytical and empirical estimations for incident blast pressure. *KSCE Journal of Civil Engineering* 21(6): 2211–2225.

US Army Corps of Engineers (1990) *TM5-1300, Structures to Resist the Effects of Accidental Explosions*. Washington, DC: US Army Corps of Engineers.

US Department of Defence (2008) *UFC 3-340-02, Structures to Resist the Effects of Accidental Explosions*. Washington DC: US Department of Defence.

US General Services Administration (2004) *Oklahoma City Federal Building*. Washington DC: GSA.

von Rosen B, Guilbeault R and Contestabile E (2004) *A Preliminary Investigation into the Propagation of Shock Waves Behind a Simple Rectangular Structure*. Bad Reichenhall, Germany: MABS18.

Wager P (2005) *Shock User's Manual Version 1.0*. Port Hueneme, CA: Naval Facilities Engineering Service Center.

Wan Q and Eliasson V (2015) Numerical study of shock wave attenuation in two-dimensional ducts using solid obstacles: how to utilize shock focusing techniques to attenuate shock waves. *Aerospace* 2: 203–221.

Warnstedt P and Gebbeken N (2020) Innovative protection of urban areas –experimental research on the blast mitigating potential of hedges. *Landscape and Urban Planning* 202: 103876.

Whitham GB (1957) A new approach to problems of shock dynamics Part 2. Three-dimensional problems. *Journal of Fluid Mechanics* 5: 369–386.

Xiao W, Andrae M and Gebbeken N (2018) Experimental and numerical investigations of shock wave attenuation effects using protective barriers made of steel posts. *Journal of Structural Engineering* 144(11): 04018204.

Xiao W, Andrae M and Gebbeken N (2019) Experimental and numerical investigations on the shock wave attenuation performance of blast walls with a canopy on top. *International Journal of Impact Engineering* 131: 123–139.

Xiao W, Andrae M and Gebbeken N (2020a) Numerical study of blast mitigation effect of innovative barriers using woven wire mesh. *Engineering Structures* 213.

Xiao W, Andrae M and Gebbeken N (2020b) Numerical study on impulse reduction performance of protective barriers made of steel posts. *Journal of Structural Engineering (United States)* 146: 1–13.

Xiao W, Andrae M, Steyerer M, et al. (2021) Investigations of blast loads on a two-storeyed building with a gable roof: Full-scale experiments and numerical study. *Journal of Building Engineering* 43: 103111.

Zhang J, Li Y, Zhao T, et al. (2021) Machine-learning based design of digital materials for elastic wave control. *Extreme Mechanics Letters* 48: 101372.

Zhi X-d, Qi S-b and Fan F (2019) Temporal and spatial pressure distribution characteristics of hemispherical shell structure subjected to external explosion. *Thin-Walled Structures* 137: 472–486.

Zhou X Q and Hao H (2008) Prediction of airblast loads on structures behind a protective barrier. *International Journal of Impact Engineering* 35(5): 363–375.

Zong R, Hao H and Shi Y (2017) Development of a new fence type blast wall for blast protection: Numerical analysis. *International Journal of Structural Stability and Dynamics* 17(6).